Journal of Computational Applied Mechanics 2025, 56(1): 222-248

DOI: 10.22059/jcamech.2025.386451.1307

RESEARCH PAPER

Physics-informed neural network for bending analysis of two-dimensional functionally graded nano-beams based on nonlocal strain gradient theory

Saba Sadat Mirsadeghi Esfahani [a], Ali Fallah [b,c,*], Mohammad Mohamadi Aghdam [a]

[a] *Mechanical Engineering Department, Amirkabir University of Technology, Tehran 15875-4413, Iran*
[b] *Faculty of Engineering and Natural Science, Sabanci University, Istanbul 34906, Turkey*
[c] *Department of Automotive Engineering, Atilim University, Ankara, 06830, Turkey*

Abstract

This paper presents the bending analysis of two-dimensionally functionally graded (2D FG) nano-beams using a physics-informed neural network (PINN) approach. The material properties of the nanobeams vary along their length and thickness directions, governed by a power-law function. Hamilton's principle, combined with the nonlocal strain gradient theory (NSGT) and Euler-Bernoulli beam theory, is employed to derive the governing equation for the bending analysis of 2D FG nanobeams. Due to the incorporation of size dependency and the variation of material properties in two dimensions, the governing equation becomes a high-order variable-coefficient differential equation, which is challenging, if not impossible, to solve analytically. In this study, the applicability of PINN for solving such high-order complex differential equations is investigated, with potential applications in nanomechanical engineering. In the PINN approach, a deep feedforward neural network is utilized to predict the mechanical response of the beam. Spatial coordinates serve as inputs, and a loss function is formulated based on the governing equation and boundary conditions of the problem. This loss function is minimized through the training process of the neural network. The accuracy of the PINN results is validated by comparing them with available reference solutions. Additionally, the effects of material distribution, power-law index (in both length and thickness directions), nonlocal strain gradient parameters, and material length scale parameters are investigated. This study demonstrates the versatility of the PINN approach as a robust tool for solving high-order differential equations in structural mechanics.

Keywords: Physics informed neural networks; Two-dimensional FG nano-beams; Bending analysis; Nonlocal strain gradient theory.

1. Introduction

Heterogeneous materials and their applications in various engineering aspects have a relatively long history.

* Corresponding author. *E-mail address: ali.fallah.66@gmail.com*

Mechanical response of these materials in practice can be determined based on their governing partial differential equations. Functionally graded materials (FGMs) constitute a novel category of heterogeneous materials characterized by their mechanical properties continuously varying across the domain. The micro-structures of the FG materials gradually shift from one material to another incorporating a specific gradient that serves to mitigate stress and strain concentration [1]. The impact of size-dependency on mechanical behavior in micro/nano systems is notable, as it requires that the stress field at a specific point is affected by both local and global strains. Micro-scaled functionally graded materials are commonly applied in NEMS and MEMS, highlighting the significance of understanding the static and dynamic behaviors of small-scale structures. Some of mechanical behaviors of nano nano FGM structures literature is reviewed: Arabzadeh-Ziari et al. [2] studied the investigate deflection, buckling and vibration for a five-layer sandwich nanocomposite beam, with reinforcements of graphene platelets (GPLs) and shape memory alloys (SMAs), and a foam core using third order shear deformation beam theory and resulted that by increasing the volume fraction of GPL from 0 to 0.03, the deflection of the beam decreases by 44%. Monajemi et al. [3] analyses the dynamic response of spinning nanocomposite sandwich cylindrical shells with a magnetorheological elastomer (MRE) core, reinforced by functionally graded polymeric laminates (FG GPLs). It considers the effects of thermomechanical loading, residual stress, spinning speed, and material properties on the shell's behavior using DQM methodology. Shirdelan et al. [4] employs the fourth-order shear deformation theory to model the control vibration of a micro-composite sandwich shell. The results demonstrate that the honeycomb core effectively reduces vibrations, and the distribution of graphene has a significant effect on the natural frequencies.

Mohammadimehr [5] examines the vibration behaviour of Timoshenko sandwich beams with porous cores and functionally graded facesheets. Combining nonlocal stress and strain elasticity concepts, the analysis explores their effects at micro/nano scales. The findings demonstrate that natural frequency decreases with higher nonlocal stress parameters and increases with higher nonlocal strain parameters, impacting beam stiffness.

There are two prominent theories in the literature to consider size-dependency in structures; i.e. nonlocal elasticity and strain gradient models [6]. For instance, Nejad et al. [7] examined the buckling behavior of a two-directional FG Euler–Bernoulli nano-beam by nonlocal elasticity theory. Their findings underscored the substantial impact of nonlocality on the mechanical properties of micro-FG beams. Similarly, Reddy et al. [8] explored bending, buckling, vibration and related issues in FG Euler–Bernoulli and Timoshenko beams, employing the modified version of couple stress theory. Nonlocal strain gradient (NSG) models have been utilized to explore the size-dependent effects on various phenomena such as bending, buckling, wave propagation, vibration and behaviors observed in small-scale structures [9-11]. Based on this theorem, stress in small scaled materials is affected by both the nonlocal stress field and the strain gradient stress field [12]. Li et al. [13, 14] studied bending, buckling and free vibration behavior of structures made of FG materials (variation through thickness) and investigated the size-dependent effects on their behavior. Most of the available research is focused on FG beams with properties varying through-thickness [11]. However, FG structures with material properties varying in two or three dimensions perform more effectively than conventional one-directional FG structures. This is because their material properties can be tailored in multiple directions to achieve specific goals. In such cases, the coefficients of the governing differential equations are no longer constant; they depend on spatial coordinates, making the equations more complex. Finding an analytical solution for this type of differential equation is challenging, if not impossible. Therefore, employing an appropriate numerical technique such as Generalized Differential Quadrature (GDQ), finite element, or finite difference (FDM) methods is crucial. However, these well-known numerical methods have inherent limitations. For example, while FDM [15] is effective for solving strong-form differential equations, it may be constrained by complex geometries, or GDQ, though robust, can encounter stability issues when dealing with intricate geometries [16].

In recent years, a variety of data-driven, deep learning and neural networks methodologies have been utilized to address governing differential equations across diverse domains including engineering, sociology, speech recognition and image processing. A notable data-driven and mesh-free technique known as PINN [17, 18], is a specialized subset of deep learning algorithms designed specifically for solving ordinary differential equations (ODEs) and partial differential equations (PDEs). By minimizing a loss function within a PINN, solutions to ODEs and PDEs are approximated through the utilization of neural networks (NN). PINNs have been successfully used for solving Burger's equation, Navier–Stokes equation [19], Cahn–Hilliard and Allen–Cahn equation [20] and the results were quite satisfying. For example, Haghighat et al. [21] figured out that PINN is compatible with FEM using results of a two-dimensional linear elasticity problems. Wu et al. [22] studied elastoplasticity issues using PINN within a heterogeneous medium exposed to random fatigue cyclic loadings. However, there are a few studies in literature that used PINN for structural analysis. For instance, Fallah et al. [1] used PINN to solve bending, free vibration of a 3D FGM porous beam resting on elastic foundation and the network hyper-parameters are tuned by a systematic optimization procedure by using Taguchi design of experiments combined with grey relational analysis. Bazmara et

al. [23] also utilized PINN to investigate nonlinear bending of 3D functionally graded beams and resulted that PINN is 71 times faster than GDQM. Zhuang and colleagues [24] employed the PINN in the energy method to analyze various characteristics of Kirchhoff plates in which a novel activation function ensures continuity and stability. Implemented in PyTorch with transfer learning, DAEM demonstrates efficient and accurate performance across various geometries, loads, and boundary conditions. Kianian et al. [25] investigated the linear bending of nano-beam on nonlinear elastic foundation combining Euler–Bernoulli beam theory and Eringen's nonlocal continuum theory, Results validate the accuracy and efficiency of PINNs through comparisons with existing literature. Recently, Eshaghi et. al [26] introduced a framework, named DeepNetBeam (DNB), based on different form of PINN for the analysis of functionally graded (FG) porous beams. The findings suggest that PINN is suitable for solving differential equations in structural engineering and nano mechanics and its predictions align closely with FE results.

In this study, the bending behavior of a 2D FG nanobeam is analyzed using the PINN method. The material properties are assumed to vary bidirectionally, along with both the length and thickness of the beam. Size dependency, a key characteristic observed in nanostructures, is incorporated into the model using the nonlocal strain gradient theory. The governing equation for the bending of size-dependent 2D FG beams is derived using Hamilton's principle in conjunction with the Euler-Bernoulli beam theory. The inclusion of size dependency and bidirectional material variation results in a high-order differential equation with variable coefficients, which is generally challenging, if not impossible, to solve analytically. In such cases, numerical techniques become indispensable.

PINN has recently demonstrated significant potential in solving various types of differential equations across diverse applications. In this study, the applicability of PINN for solving the high-order variable-coefficient differential equations encountered in structural nano-mechanics is explored. In the PINN framework, a neural network is employed to predict the beam's deflection, with its parameters optimized through the minimization of a loss function. The physics of the problem, represented by the governing equation and corresponding boundary conditions, is embedded into this loss function.

The accuracy of PINN predictions is validated through comparisons with analytical and numerical reference solutions. The results reveal that PINN can accurately predict the bending behavior of 2D FG beams under various loading scenarios and boundary conditions. The study also investigates the effects of material variability, different loading conditions, length scale parameters, and nonlocal effects. These findings have significant implications for the design and analysis of functionally graded nanobeams in engineering applications such as nano-structural components, sensors, and actuators, where high sensitivity and optimal performance are critical. The developed PINN framework demonstrates its potential as a robust tool for addressing complex bending problems in materials with spatially varying properties.

2. Mathematical modelling

2.1. Two dimensional Functionally Graded Beam

Figure 1 shows a size-dependent two-dimensional FG beam with geometric parameters, width *b*, thickness *h* and length *L*.

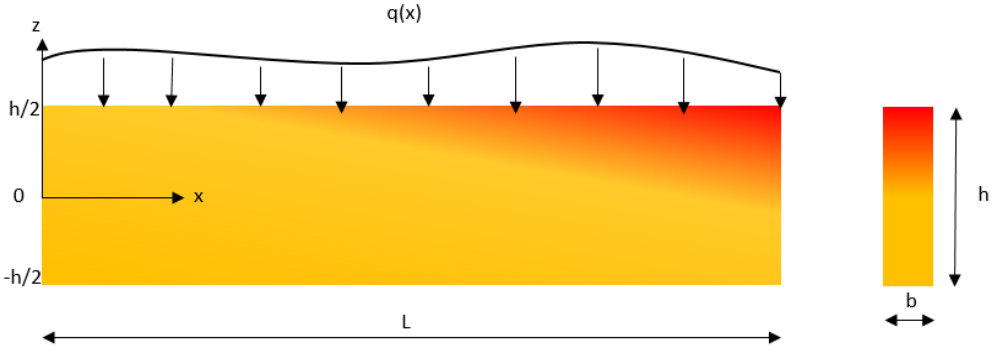

Figure 1. Schematic figure of Two dimensionally FG nanobeam

The material properties of the nano-beam are assumed to vary continuously along its length and thickness based on a power-law distribution. The Euler-Bernoulli theory of beams is assumed. In this study small deformation theory

is applied, implying that the analysis does not account for geometric nonlinearities. Axial displacement deformations are neglected in further explanation of this chapter. This study is limited to 2D FGM nano-beam, despite the literature which is mostly 1d FGM through length. However, 3d effects or complex geometries is neglected.

The FG beam is composed of two distinct materials, i.e. metal and ceramic and the effective material properties, such as Young's modulus (E) and density (ρ), vary continuously along the length and thickness of the beam in accordance with the rule of mixture as [27, 28]:

$$E(x,z) = ((E_m - E_c)\left(\frac{x}{L}\right)^k \left(\frac{z}{h}+\frac{1}{2}\right)^{\beta} + E_c)$$
$$\rho(x,z) = ((\rho_m - \rho_c)\left(\frac{x}{L}\right)^k \left(\frac{z}{h}+\frac{1}{2}\right)^{\beta} + \rho_c) \quad (1)$$

where m and c sub index represent the metal and ceramic material, respectively. Moreover, non-negative parameters k, β serve as the power-law index, characterizing the material variation profile across the length and thickness and indicating microstructure of the 2D FG nano-beam. Power law indices, k and β, directly influence both modulus of elasticity and density of the beam. Figure 2 and Figure 3 show the effects of power low indices on the variations of Young's modulus and density across the dimensionless length ($\overline{X} = \frac{x}{L}$) and thickness ($\overline{Z} = \frac{z}{h}$) of the beam. As shown in the following figures, properties of the beam start from ceramic part ($E = E_c$ and $\rho = \rho_c$) at left-bottom corner and gradually changes to metal at top-right corner.

Based on the Euler-Bernoulli beam theory, one may consider displacement fields as:

$$U(x,z,t) = u(x,t) - z\frac{\partial w}{\partial x}$$
$$V(x,z,t) = 0 \quad (2)$$
$$W(x,z,t) = w(x,t)$$

Here U, V, W represent displacement components along the x; y and z directions, respectively and u and w are the axial and transverse displacement of a point on the center line of the beam. Consequently, the non-zero linear strains can be written as [27]:

$$\varepsilon_{xx} = \frac{\partial u}{\partial x} - z\frac{\partial^2 w}{\partial x^2} \quad (3)$$

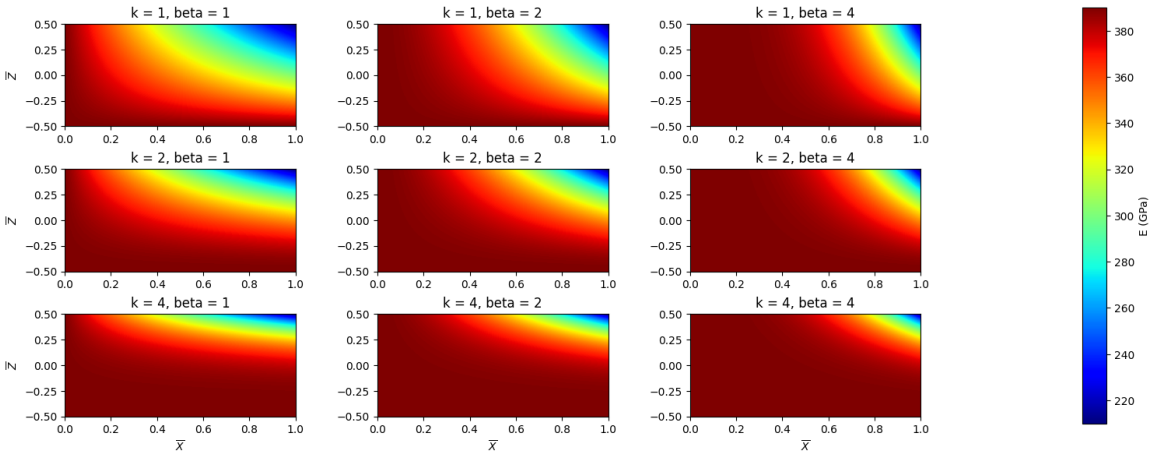

Figure 2.Variation of modulus of elasticity vs. dimensionless length and thickness for various power low indices

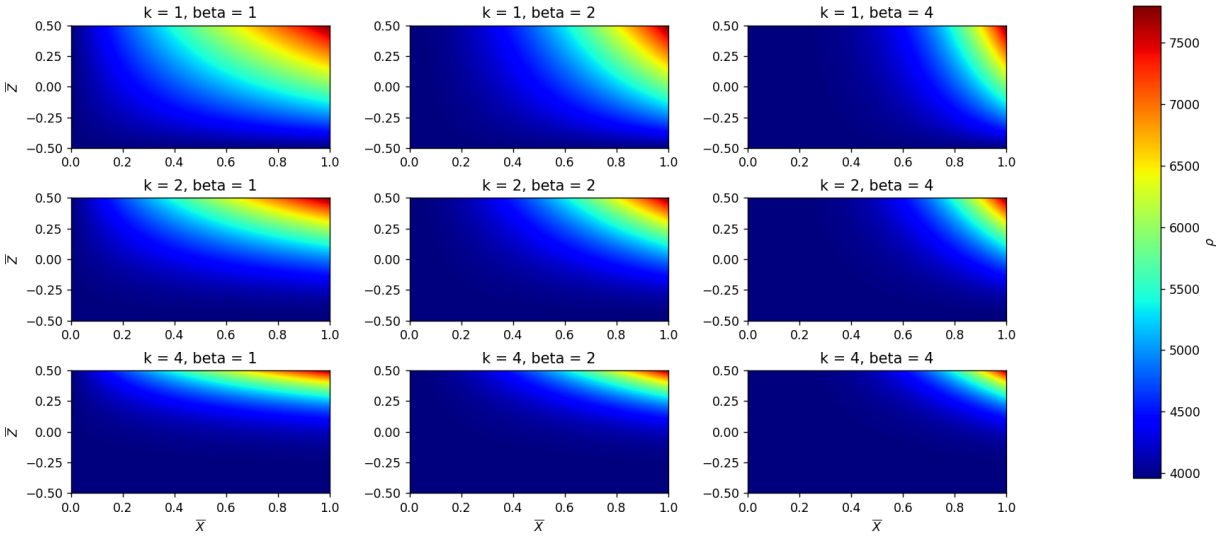

Figure 3. Variation of density vs. dimensionless length and thickness for various power low indices

2.2. Nonlocal Strain Gradient Theory

In order to include size dependency into classical elasticity theory, various theories have been proposed by researchers. Among these theories, one may refer to the nonlocal strain gradient theory in which a combination of the effects of strain gradients and nonlocal interactions is considered. Based on this theory, the total stress can be expressed as [29]:

$$t_{xx} = \sigma_{xx} - \frac{d\sigma_{xx}^{(1)}}{dx} \tag{4}$$

in which σ_{xx} denotes classical stress term and $\sigma_{xx}^{(1)}$ refers to the higher-order stress as:

$$\sigma_{xx} = \int_0^L E(x,z)\alpha(x,x',ea)\varepsilon'_{xx}(x')dx' \tag{5}$$

$$\sigma_{xx}{}^{(1)} = l^2 \int_0^L E(x,z)\alpha(x,x',ea)\varepsilon'_{xx,x}(x')dx' \tag{6}$$

where l is the material length scale parameter and shows the importance of strain gradient stress field [30], ea is the nonlocal parameter, L is the length of the beam and the nonlocal kernel function $\alpha(x,x',ea)$ satisfies the conditions developed by Eringen [6]. For the sake of simplicity, Li et al [27] suggested that instead of Eqs. (5) and (6), the differential form of the equations can be used as:

$$(1-(ea)^2\nabla^2)\sigma_{xx} = E(x,z)\varepsilon_{xx} \tag{7}$$

$$(1-(ea)^2\nabla^2)\sigma_{xx}{}^{(1)} = l^2 E(x,z)\varepsilon_{xx,x} \tag{8}$$

Combining Eqs. (4), (7) and (8), one can rewrite the total stress relation based on the nonlocal strain gradient theory as:

$$(1-(ea)^2\nabla^2)t_{xx} = E(x,z)\varepsilon_{xx} - l^2\nabla.(E(x,z)\nabla\varepsilon_{xx}) \tag{9}$$

It should be noted that Eq. (9) can be divided into two case studies; l = 0 and ea = 0 which respectively represents nonlocal continuum theory and strain gradient theory [31].

2.3. Governing equations

Considering the Euler–Bernoulli and the nonlocal strain gradient theories together with Hamilton's principle

within the two dimensional domain of the beam; $0 < x < L$ and $-\frac{h}{2} < z < \frac{h}{2}$, one can derive the governing equations for the 2D FG nano-beams as [27]:

$$\delta u : \frac{\partial N_{xx}}{\partial x} - f = 0 \tag{10}$$

$$\delta w : \frac{\partial^2 M_{xx}}{\partial x^2} - \overline{N}\frac{\partial^2 w}{\partial x^2} = q \tag{11}$$

where q and f are the applied external distributed load in transverse and axial direction, respectively and $\overline{N}$ denotes the axial compressive force. The N_{xx} is axial force resultant, M_{xx} is the bending moment resultant. Considering the Eq. (9) and the equilibrium equations, after some mathematical simplifications, it is possible to derive force and bending moment resultants of the FG beam as:

$$N_{xx} = (ea)^2 \frac{\partial^2 N_{xx}}{\partial x^2} + A_{11}\frac{\partial u}{\partial x} - B_{11}\frac{\partial^2 w}{\partial x^2} - l^2\left(A_{11}\frac{\partial^3 u}{\partial x^3} - B_{11}\frac{\partial^4 w}{\partial x^4} + \frac{\partial A_{11}}{\partial x}\frac{\partial^2 u}{\partial x^2} - \frac{\partial B_{11}}{\partial x}\frac{\partial^3 w}{\partial x^3}\right) \tag{12}$$

$$M_{xx} = (ea)^2 \frac{\partial^2 M_{xx}}{\partial x^2} + B_{11}\frac{\partial u}{\partial x} - D_{11}\frac{\partial^2 w}{\partial x^2} - l^2\left(B_{11}\frac{\partial^3 u}{\partial x^3} - D_{11}\frac{\partial^4 w}{\partial x^4} + \frac{\partial B_{11}}{\partial x}\frac{\partial^2 u}{\partial x^2} - \frac{\partial D_{11}}{\partial x}\frac{\partial^3 w}{\partial x^3}\right) \tag{13}$$

The procedure to obtain Eqs. (12) and (13) is obtained in Appendix A In which stiffness coefficients are defined as:

$$\begin{aligned} A_{11}(x) &= \int E(x,z)\,dzdy \\ B_{11}(x) &= \int zE(x,z)\,dzdy \\ D_{11}(x) &= \int z^2 E(x,z)\,dzdy \end{aligned} \tag{14}$$

Where $A_{11}(x)$ is tension-compression stiffness, $B_{11}(x)$ is tension-bending coupling term, $D_{11}(x)$ is the bending stiffness. It should be noted that all these coefficients are functions of x and vary along the beam length. By substitution of the N_{xx} and M_{xx} resultants into the equilibrium Eqs. (10) and (11),the governing equations for the size-dependent 2D FG beams based on the nonlocal strain gradient theory can be derived as:

$$\delta u : \left(1-(ea)^2\frac{\partial^2}{\partial x^2}\right)(-f) + \frac{\partial}{\partial x}\left(A_{11}\frac{\partial u}{\partial x} - B_{11}\frac{\partial^2 w}{\partial x^2} - l^2\left(A_{11}\frac{\partial^3 u}{\partial x^3} - B_{11}\frac{\partial^4 w}{\partial x^4} + \frac{\partial A_{11}}{\partial x}\frac{\partial^2 u}{\partial x^2} - \frac{\partial B_{11}}{\partial x}\frac{\partial^3 w}{\partial x^3}\right)\right) = 0 \tag{15}$$

$$\delta w : -\left(1-(ea)^2\frac{\partial^2}{\partial x^2}\right)\left(\overline{N}\frac{\partial^2 w}{\partial x^2} + q\right) + \frac{\partial^2}{\partial x^2}\left(B_{11}\frac{\partial u}{\partial x} - D_{11}\frac{\partial^2 w}{\partial x^2} - l^2\left(B_{11}\frac{\partial^3 u}{\partial x^3} - D_{11}\frac{\partial^4 w}{\partial x^4} + \frac{\partial B_{11}}{\partial x}\frac{\partial^2 u}{\partial x^2} - \frac{\partial D_{11}}{\partial x}\frac{\partial^3 w}{\partial x^3}\right)\right) = 0 \tag{16}$$

The process for obtaining Eqs. (15) and (16) is outlined in Appendix B. The Eqs. (15) and (16) are two coupled partial differential equations with variable coefficients which is the most general form of governing equation for a size dependent beam. It is possible to reach to the governing equation for special cases by simplifying this equation. For instance, by letting $ea=l=0$, the governing equation for 2D FG beam based the classical theory is obtained as:

$$A_{11}\frac{\partial^2 u}{\partial x^2} + \frac{\partial A_{11}}{\partial x}\frac{\partial u}{\partial x} - B_{11}\frac{\partial^3 w}{\partial x^3} - \frac{\partial B_{11}}{\partial x}\frac{\partial^2 w}{\partial x^2} - f = 0 \tag{17}$$

$$B_{11}\frac{\partial^3 u}{\partial x^3} + 2\frac{\partial B_{11}}{\partial x}\frac{\partial^2 u}{\partial x^2} + \frac{\partial^2 B_{11}}{\partial x^2}\frac{\partial u}{\partial x} - D_{11}\frac{\partial^4 w}{\partial x^4} - 2\frac{\partial D_{11}}{\partial x}\frac{\partial^3 w}{\partial x^3} - \frac{\partial^2 D_{11}}{\partial x^2}\frac{\partial^2 w}{\partial x^2} - \overline{N}\frac{\partial^2 w}{\partial x^2} - q = 0 \tag{18}$$

Moreover, assuming that the material properties are homogeneous, the governing equation for homogeneous beam based on the nonlocal strain gradient theory can be obtained as:

$$l^2 A_{11}\frac{\partial^4 u}{\partial x^4}+A_{11}\frac{\partial^2 u}{\partial x^2}-\left(1-(ea)^2\frac{\partial^2}{\partial x^2}\right)f=0 \tag{19}$$

$$l^2 D_{11}\frac{\partial^6 w}{\partial x^6}-D_{11}\frac{\partial^4 w}{\partial x^4}-\left(1-(ea)^2\frac{\partial^2}{\partial x^2}\right)\left(\overline{N}\frac{\partial^2 w}{\partial x^2}+q\right)=0 \tag{20}$$

Since the material properties are not uniform in the *z* direction, the axial-bending coupling term, $B_{11}(x)$ is not zero resulting the axial and transvers deflection to be coupled, despite the homogeneous case. It is possible to shift the reference line from the center line of the beam to the physical neutral axis to decouple these deformations. To this end, one may use the method suggested by Abrate [32] and Luo [33] to define reference point as $z=z'+\delta$, with $\delta=\frac{B_{11}}{A_{11}}$ to achieve $B_{11}{}'=0$ and decouple equations. Considering this new reference point, other stiffness components are defined as, $D_{11}{}'=D_{11}-\frac{(B_{11})^2}{A_{11}}$ and $A_{11}{}'=A_{11}$. Thus, the governing Eqs. (15) and (16) reduces as:

$$\delta u:-\left(1-(ea)^2\frac{\partial^2}{\partial x^2}\right)f+\frac{\partial}{\partial x}\left(A'_{11}\frac{\partial u}{\partial x}-l^2\left(A'_{11}\frac{\partial^3 u}{\partial x^3}+\frac{\partial A'_{11}}{\partial x}\frac{\partial^2 u}{\partial x^2}\right)\right)=0 \tag{21}$$

$$\delta w:-\left(1-(ea)^2\frac{\partial^2}{\partial x^2}\right)\left(\overline{N}\frac{\partial^2 w}{\partial x^2}+q\right)+\frac{\partial^2}{\partial x^2}\left(-D'_{11}\frac{\partial^2 w}{\partial x^2}-l^2\left(-D'_{11}\frac{\partial^4 w}{\partial x^4}-\frac{\partial D'_{11}}{\partial x}\frac{\partial^3 w}{\partial x^3}\right)\right)=0 \tag{22}$$

In this new form, the deformations in the transvers and axial directions are decoupled and can be investigated separately. It is known that in the bending of beams, the axial displacement is negligible compared to the transverse displacement [34, 35], thus in continue only the transvers displacement is considered and studied.

The bending moment resultant is also reducing to:

$$M_{xx}=(ea)^2\left(\overline{N}\frac{\partial^2 w}{\partial x^2}+q\right)-D'_{11}\frac{\partial^2 w}{\partial x^2}+l^2\left(D'_{11}\frac{\partial^4 w}{\partial x^4}+\frac{\partial D'_{11}}{\partial x}\frac{\partial^3 w}{\partial x^3}\right) \tag{23}$$

For the sake of generality, the following dimensionless parameters are defined as:

$$\overline{W}=\frac{w}{L},\ \overline{X}=\frac{x}{L},\ \tau=\frac{ea}{L},\ \zeta=\frac{l}{L},\ \bar{q}=\frac{qL^3}{D_{00}},\ m_{xx}=\frac{M_{xx}L}{D_{00}},\ d_{11}{}'=\frac{D_{11}{}'}{D_{00}} \tag{24}$$

In which $D_{00}=I_0E_c$. The non-dimensional form of governing transverse equation of 2D FG beam based on the nonlocal-strain gradient theory can be written as:

$$\zeta^2 d_{11}{}'\frac{\partial^6\overline{W}}{\partial\overline{X}^6}+3\zeta^2\frac{\partial d_{11}{}'}{\partial\overline{X}}\frac{\partial^5\overline{W}}{\partial\overline{X}^5}+\left(3\zeta^2\frac{\partial^2 d_{11}{}'}{\partial\overline{X}^2}-d_{11}{}'\right)\frac{\partial^4\overline{W}}{\partial\overline{X}^4}+\left(\zeta^2\frac{\partial^3 d_{11}{}'}{\partial\overline{X}^3}-2\frac{\partial d_{11}{}'}{\partial\overline{X}}\right)\frac{\partial^3\overline{W}}{\partial\overline{X}^3} \tag{25}$$
$$-\frac{\partial^2 d_{11}{}'}{\partial\overline{X}^2}\frac{\partial^2\overline{W}}{\partial\overline{X}^2}-\tau^2\frac{\partial^2\bar{q}}{\partial\overline{X}^2}+\bar{q}=0$$

The dimensionless bending moment resultant is also derived as:

$$m_{xx}=\tau^2\bar{q}-d_{11}{}'\frac{\partial^2\overline{W}}{\partial\overline{X}^2}+\zeta^2\left(d_{11}{}'\frac{\partial^4\overline{W}}{\partial\overline{X}^4}+\frac{\partial d_{11}{}'}{\partial\overline{X}}\frac{\partial^3\overline{W}}{\partial\overline{X}^3}\right) \tag{26}$$

Utilizing the nonlocal strain gradient theory may lead to insufficiencies in conventional boundary conditions due to the higher order of the differential equations.

Consequently, an additional boundary condition known as the non-classical boundary condition is introduced for use in nonlocal strain gradient models as [23]:

$$\frac{\partial^2 \overline{W}}{\partial \overline{X}^2} = 0 \tag{27}$$

Table 1 provides other well-known conventional boundary conditions for free, simply supported and clamped edges.

Table 1. Different types of classical boundary conditions

Type of boundary condition	Constrained items	Number Equation
Free edge	$\frac{\partial m_{xx}}{\partial \overline{X}} = 0, m_{xx} = 0$	(28)
Clamped edge	$\overline{W} = 0, \frac{\partial \overline{W}}{\partial \overline{X}} = 0$	(29)
Simply supported edge	$\overline{W} = 0, m_{xx} = 0$	(30)

3. Solution methodology

It should be noted that the Eq. (25) is a variable coefficient differential equation that, in general, is difficult, if not impossible, to solve analytically. Thus, application of the numerical method for solution of this equation seems necessary.

In this study, the recently developed PINN, which is a mesh-free computational method, is employed for solving the governing differential equations. PINN uses unsupervised deep learning techniques to generate solutions by training a neural network on random data points within the domain mainly to approximate the governing ordinary or partial differential equation. It should be noted that PINN does not need any labeled data. Raissi et al. [36] have demonstrated the effectiveness of the PINN approach in tackling nonlinear partial differential equations such as the Burgers, Schrödinger and Allen-Cahn equations. Besides that, results of limited available studies in the literature proved the applicability of PINN for structural analysis of beams and plates [1, 37, 38].

The general form of the time-independent differential equation and boundary conditions on the domain can be considered as [1]:

$$D\left[u(x)\right] = D\left(x; u, \frac{\partial u}{\partial x_1}, ..., \frac{\partial u}{\partial x_d}; \frac{\partial^2 u}{\partial x_1 \partial x_1}, ... \frac{\partial^2 u}{\partial x_1 \partial x_d} \right) = 0, \qquad x \in R^d \tag{31}$$

$$B_k\left[u(x)\right] = B\left(x; u, \frac{\partial u}{\partial x_1}, ..., \frac{\partial u}{\partial x_d}; \frac{\partial^2 u}{\partial x_1 \partial x_1}, ... \frac{\partial^2 u}{\partial x_1 \partial x_d} \right) = 0, \qquad \text{on } \partial\Omega \tag{32}$$

in which D is a linear or nonlinear differential operator, $u(x_i)$ is the solution function to the PDE/ODE and x_i is the general framework coordinates. B_k is the set of general boundary operator and $\partial\Omega$ is the domain's boundary which can be formed as combinations of any boundary condition such as Neumann, Dirichlet and Mixed BCs.

Based on the universal approximation theorem, a feedforward neural network with one single hidden layer is enough to approximate any continuous function [39]. For complex and nonlinear functions, the number of neurons of that hidden layer should be increased to capture the whole feature of the considered function. Another approach called deep neural network (DNN) uses more hidden layers with fewer neurons instead of just one hidden layer with a high number of neurons [40, 41]. Based on the general idea of PINN, the unknown variable i.e. $u(x_i)$ is approximated by a neural network as:

$$u(x) \cong u(x; W, b) = N^L(x; W, b) : \mathbb{R}^{d_{in}} \to \mathbb{R}^{d_{out}} \tag{33}$$

where N is an L-layer DNN (of L-1 hidden layer) with input vector x, output vector u and W, b are network parameters which are called weight matrix and bias vector, respectively. The number of neurons in the input layer, output layer and ith hidden layer are designed as d_{in}, d_{out} and N_{ni}, respectively. Various subsets of DNNs include

feedforward networks, convolutional neural networks and recurrent neural networks. Prior research has shown that feedforward neural networks (FFNN) are effective in solving PDEs/ODEs [42]. Feedforward neural network means that it is not a loop and its fully connected, in other words, every neuron is connected to the next one [39] and the data for each layer is derived from the preceding layer according to the nested equation employed in the feedforward neural network:

$$z^i = \sigma^i\left(W^i.z^{i-1} + b^i\right), i = 1,...,L \tag{34}$$

At i=0, $z^0 \equiv x$ is the model's input and at i=L, $z^L \equiv u$ which is the model's output. W^i and b^i as mentioned previously pertain to the weights matrix and biases vector of the i_{th} layer, respectively. The activation function denoted by σ plays a crucial role in connecting the input and output of each layer, various activation functions are used like: Swish, logistic sigmoid, Exponential Linear Unit (ELU), the (tanh) hyperbolic tangent, Adaptive Piecewise Linear (APL) and the rectified linear unit [42]. In this investigation, the hyperbolic tangent (tanh) is used as activation function.

The next step involves computing the derivatives of the network outputs with respect to the network inputs. In the context of PINNs, the input parameters—specifically the spatial coordinates in Cartesian coordinates—carry physical implication. Consequently, differentiating the network output with respect to these input variables also carries physical implications. Unlike traditional DNNs, where derivatives pertain to network parameters such as weights and biases during training, PINNs utilize automatic differentiation (AD), also known as algorithmic differentiation, to compute derivatives with respect to input parameters. AD has been increasingly integrated into various machine learning frameworks such as TensorFlow [43], PyTorch [44], Theano [45] and MXNet [46]. The subsequent step in PINNs involves training the network parameters by minimizing a suitable loss function that incorporates the underlying physics of the problem domain.

3.1. Training procedure and hyper parameters

In order to train the model, a group of random training points (x_t) inside the domain (x_d) and boundary (x_b) are needed. Unlike other types of neural networks, PINN does not require enormous set of data and only spatial coordinates of training points are enough [1]. To train the NN, the mean squared error (MSE) loss must be minimized:

$$L(x_t;W,b) = \omega_D L_D(x_d;W,b) + \omega_b L_b(x_b;W,b) \tag{35}$$

Where L_D and L_b are the loss functions corresponding to the governing differential equation and boundary conditions, respectively and defined as:

$$L_D(x_d;W,b) = \frac{1}{|x_d|}\sum_{x\in x_d}\left|D\left(x_d;\frac{\partial u}{\partial x_1},...,\frac{\partial u}{\partial x_d};\frac{\partial^2 u}{\partial x_1 \partial x_1},...,\frac{\partial^2 u}{\partial x_1 \partial x_d}\right)\right|^2$$
$$L_b(x_b;W,b) = \frac{1}{|x_b|}\sum_{x\in x_b}\left|B(u,x)\right|^2 \tag{36}$$

and ω_D and ω_b are the weights related to domain and boundary loss functions, respectively. In this study, weights for PDE and boundary conditions are considered equal. The outcome of the training process is the set of model parameters that minimize the loss function. Figure 4 shows the schematic of the PINN algorithm used for the solution of governing equation. Due to the nonlinearity and non-convexity of the defined loss function with respect to the model parameters, it is advisable to employ a gradient-based optimizer such as the Adam optimization scheme to minimize the loss function [1, 47].

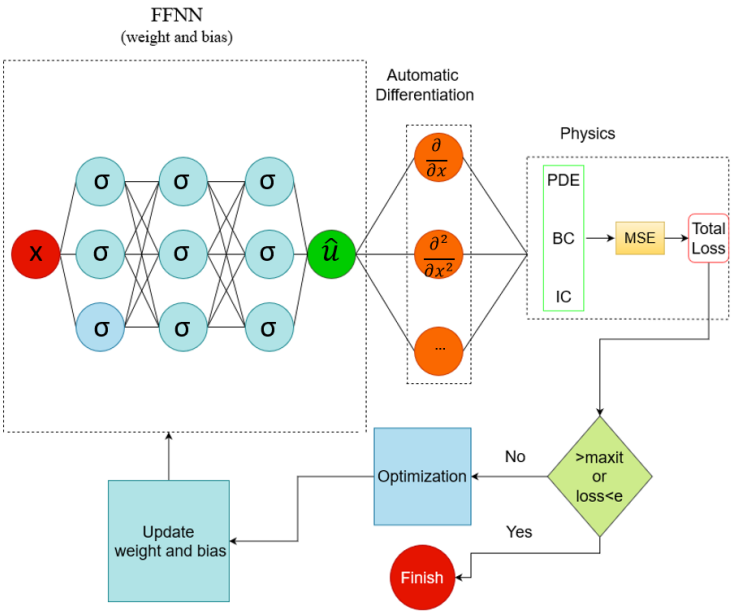

Figure 4. Schematic of PINN framework for solution of governing equation

In PINNs, the solution process involves tackling a nonconvex optimization problem rather than solving a system of algebraic or differential equations, which is typical in conventional numerical methods. Consequently, there is no guarantee of unique solutions [42]. To address this challenge, careful tuning of the model's hyper parameters is crucial. In this study following parameters employed:

- Hidden layer's neurons (N_{ni}): N_{ni} =18
- Hidden layer's number (N_H): N_H =3
- learning rate (L_R): L_R =0.001
- activation function: tanh (hyperbolic tangent)
- Optimization method: Adam
- number of training points inside the domain (N_D) and on boundary: N_D =100

Increasing the N_{ni}, N_D and epochs improves the accuracy of the results and required computational efforts and simulation time. Among available software packages for implementation of the PINN, in this study DeepXDE [42] as an easy-to-use PINN software package is employed.

4. Result and discussion

The results of bending analysis of two dimensionally FG nano-beams based on the nonlocal strain gradient theory are discussed in this section and the effects of material distribution and also the size dependency is investigated. The material parameters are extracted from Li et al. [27] to ease the comparison and validation process. In all examples, the nano-beam with following dimensional parameters is considered:

$$h = 17.6 \times 10^{-6}(m), \qquad b = 2h, \qquad L = 30h$$

Table 2-Material's property

Materials	Young's Modulus E (GPa)	Mass density ρ (kg/m^3)
Steel (metal)	210	7800
Al_2O_3 (ceramic)	390	3960

5. As the first validation attempt, Figure 5 shows the homogenous clamped-clamped beam deflection with various ζ values under uniform distributed load ($\bar{q} = 10$). It is obvious that, PINN's prediction agrees well with the exact solution. Moreover, results showed that the size dependency have important effect on the maximum deflections of the beam and by increasing material length scale parameter ζ, the maximum deflection decreases thus the bending stiffness of FG beams increases.

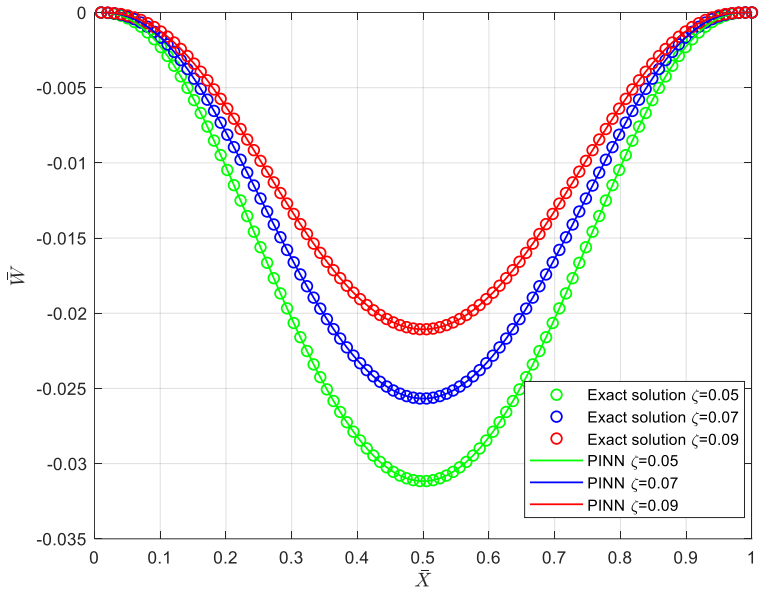

Figure 5. Dimensionless Homogenous beam deflection under uniform distributed load with clamped-clamped boundary condition for different values of material length scale parameter ζ , $\bar{q} = 10$

In another example, Figure 6 shows the simply supported homogenous beam deflection for various ζ values under sinusoidal distributed load. Figure 7.a-d show the corresponding loss function value for each ζ. The same fact is indicated that by increasing the length scale parameter the deflection is decreasing no matter what kind of distributed load is on the beam. Furthermore, the results from PINNs consistently demonstrate strong agreement with the exact solution, with the loss function decreasing rapidly to a small value. This rapid decrease indicates that PINNs can converge to an accurate solution after enough training iterations.

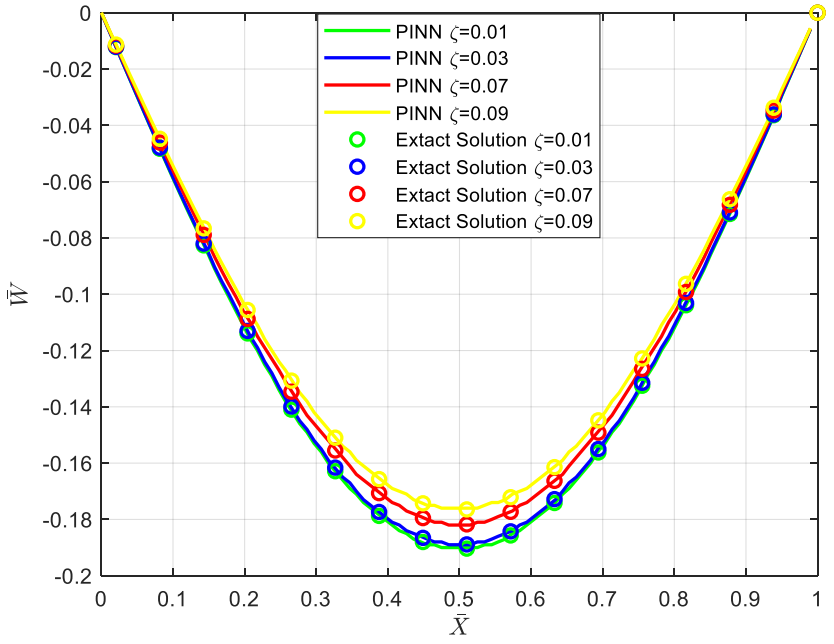

Figure 6. Deflection of homogenous beam under sinusoidal load with simply supported - simply supported boundary

condition for different values of ζ, ($\bar{q} = 10\sin(\pi x)$).

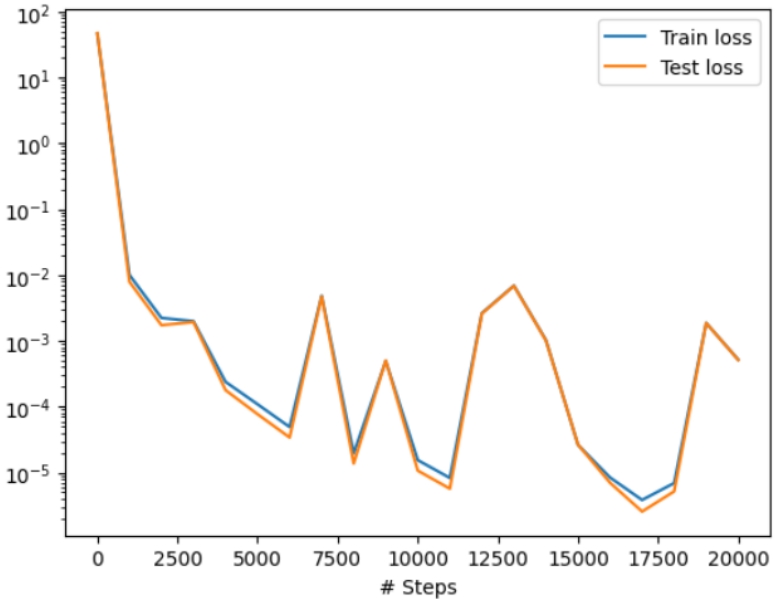

(a)

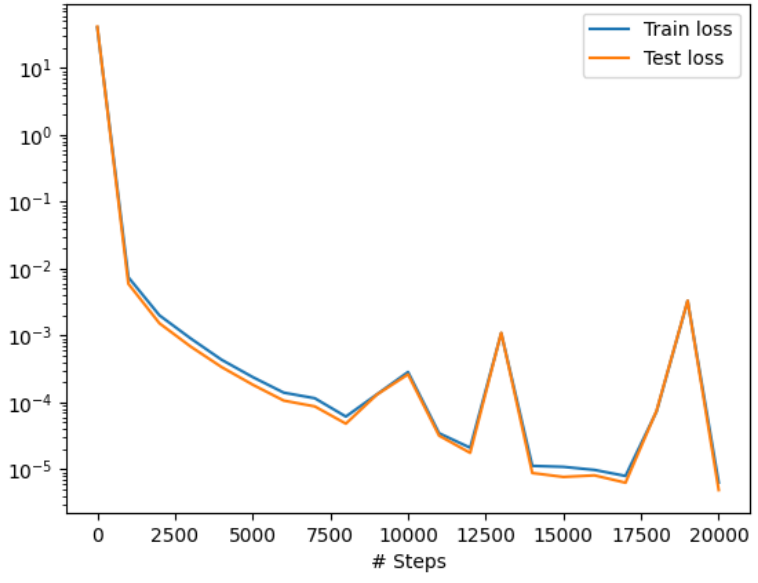

(b)

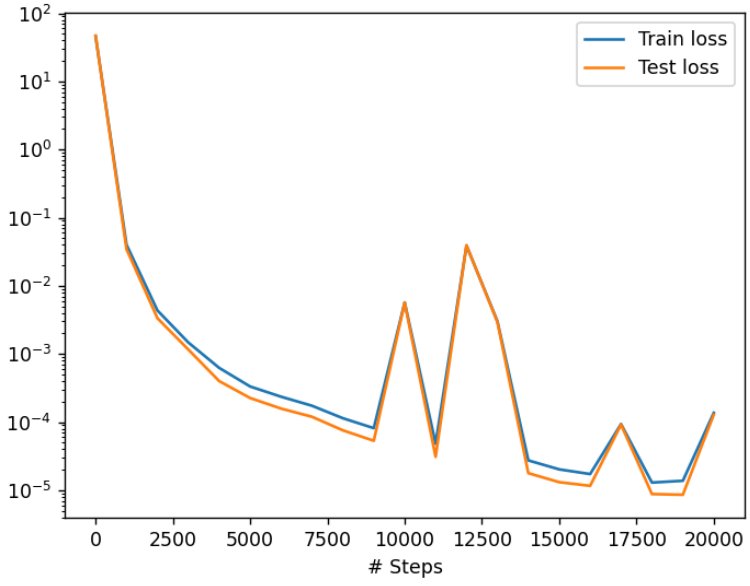

(c)

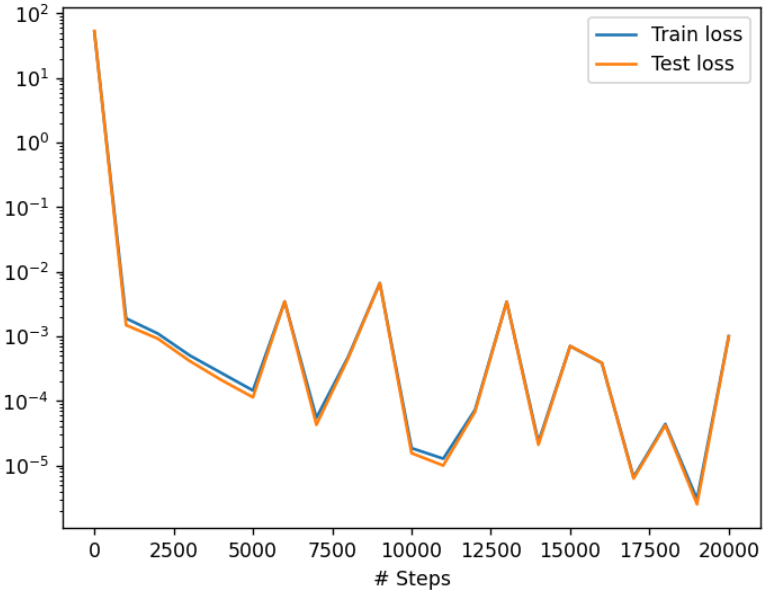

(d)

Figure 7. a) Loss function value for ζ=0.09, b) loss function value for ζ=0.07, c) loss function value for ζ=0.03, and d) loss function value for ζ=0.01.

Figure 8 shows the effect of nonlocality (τ) on deflection of homogenous beam under sinusoidal distributed load $\bar{q} = 10\sin(\pi x)$ with simply supported boundary condition. The results include the exact solution for comparison, showing good agreement with the predictions from PINNs. Consistent with prior studies, increasing the nonlocal effect renders the beam more compliant, leading to an increase in maximum deflection.

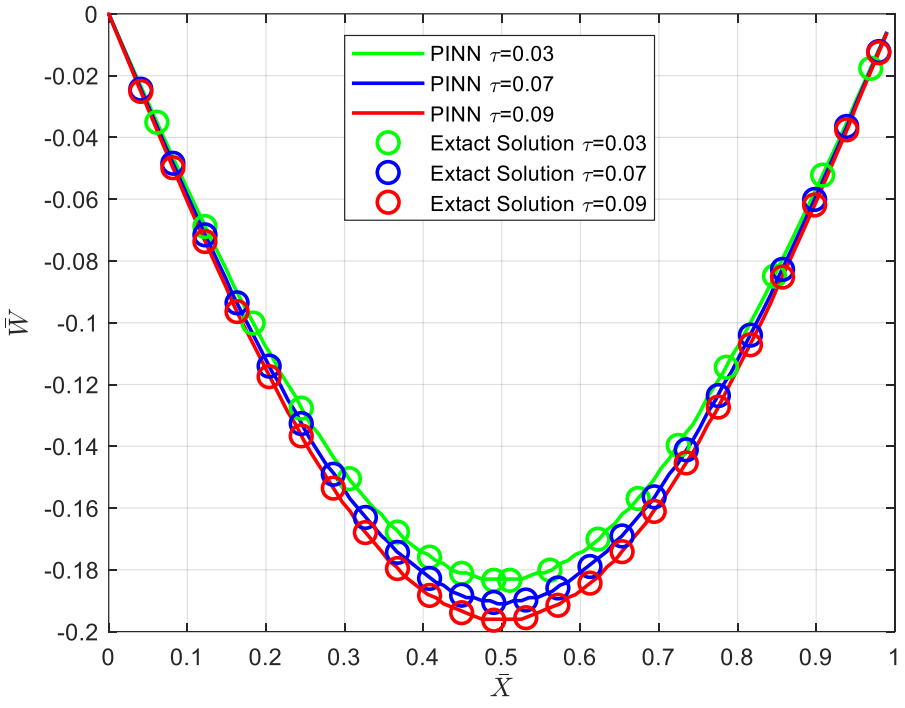

Figure 8. Deflection of homogenous beam under sinusoidal load with simply supported - simply supported boundary condition for different values of τ (ζ =0.07).

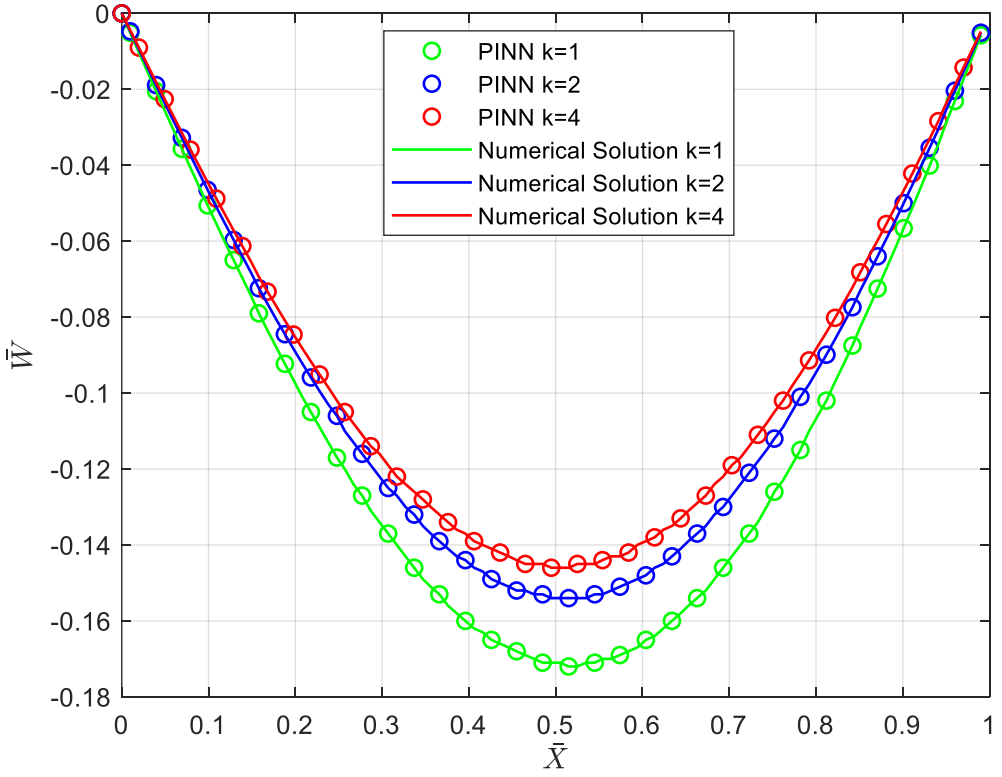

Figure 9. Deflection of axially FGM beam under uniform distributed load with simply supported-simply supported boundary condition for various power law index (*k*) values (here ζ =0.03 and $\bar{q} = 10$)

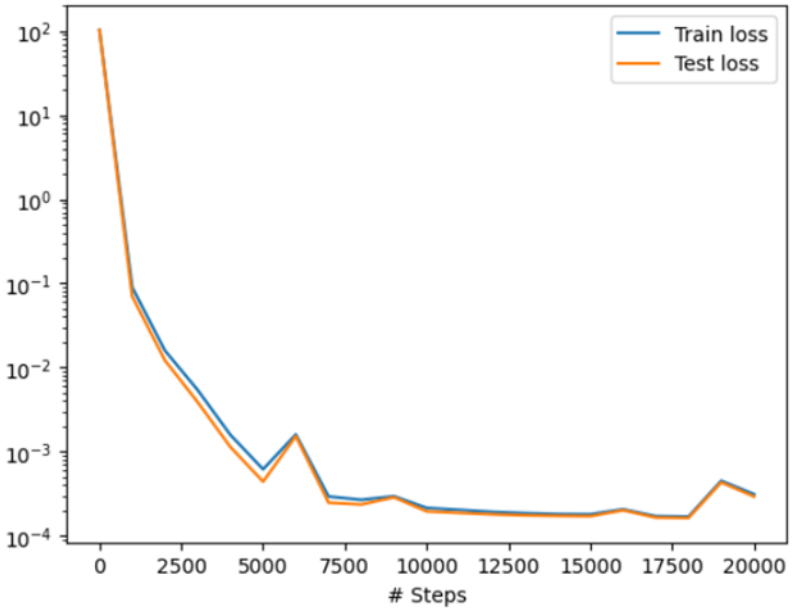
Train loss
Test loss
10^{2}
10^{1}
10^{0}
10^{-1}
10^{-2}
10^{-3}
10^{-4}
0
2500
5000
7500
10000
12500
15000
17500
20000
Steps

(a)

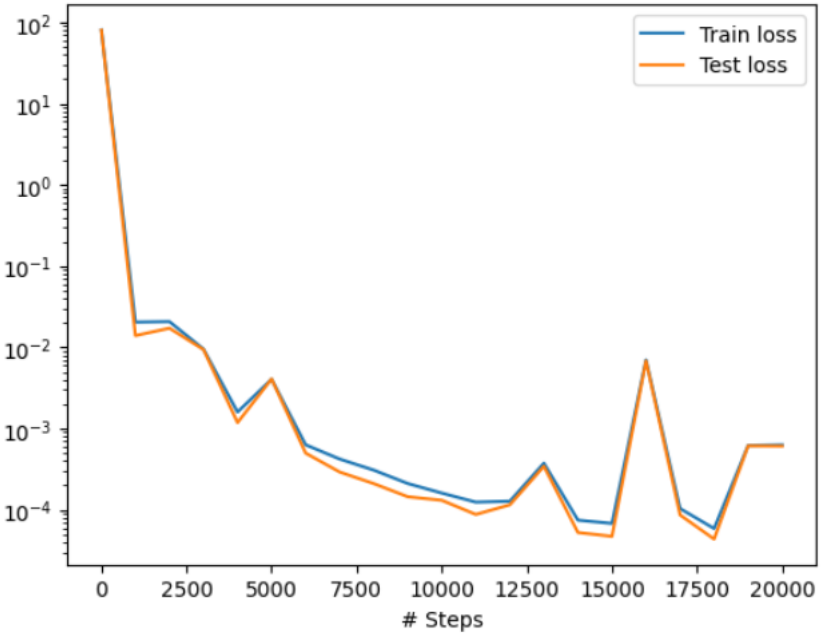
Train loss
Test loss
10^{2}
10^{1}
10^{0}
10^{-1}
10^{-2}
10^{-3}
10^{-4}
0
2500
5000
7500
10000
12500
15000
17500
20000
Steps

(b)

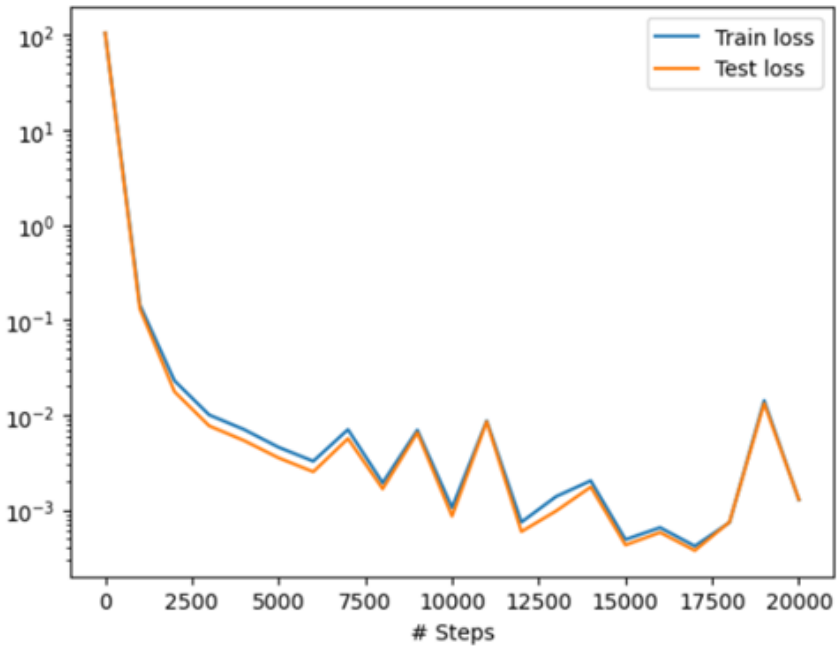

(c)

Figure 10.a. Loss function value for k=1, b) loss function value for k=2, and c) loss function value for k=4.

Figure 9 shows the deflection of axially FG nano-beam using nonlocal strain gradient beam under uniform distributed load. Results of BVP4C method in MATLAB are also used for comparison. Results showed that by increasing the power law index, the beam stiffness increases and consequently the deflection decreases. Again, there is a good agreement between the PINN predictions and the numerical solution even for this complex case. Figure 10.a, b, c shows loss function value for the considered each power law index and again it is obvious that the loss function decreases quickly during the raining procedure.

Nano-FG beam under a piecewise uniformly distributed load with simply supported ends is illustrated in Figure 11. Half of the beam is under positive and the other half is under negative uniformly distributed load with the same amplitude.

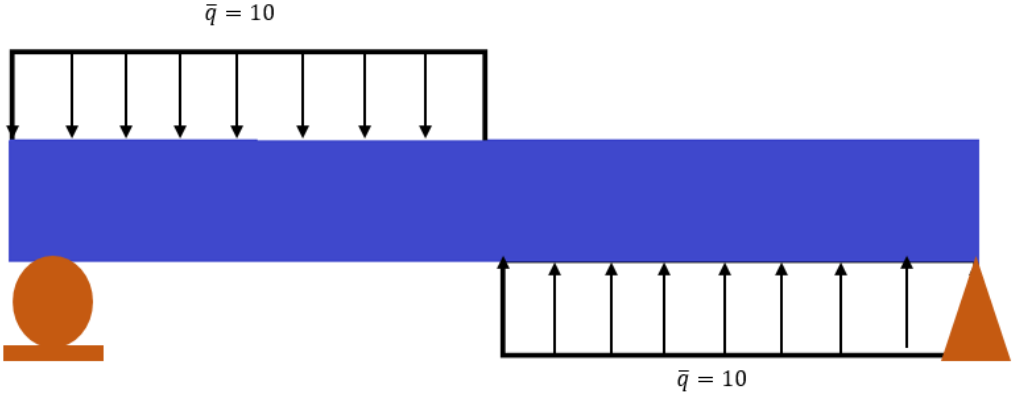

Figure 11. Nano-FGM beam with simply supported ends under piecewise uniformly distributed load, one half of beam is under positive load and the other half is under negative load.

Figure 12 shows the deflection of an axially functionally graded nano-beam with different material index (k) values under piecewise uniformly distributed load as shown in Figure 11. The case of k=0, is equal to homogenous beam, thus the deformation is symmetrical with respect the beam midpoint. However, for FG beams with $k \neq 0$ the deflection is unsymmetric due to variation in material properties along the beam length. Results of Li et al. [27] are also included for comparison which showed a good agreement with the PINN predictions. It should be noted that

the effects of variation of k on the beam deflection on the right section is more significant. It can be due to the lower stiffness of the metal side of beam (right side) compared to the ceramic section (left side).

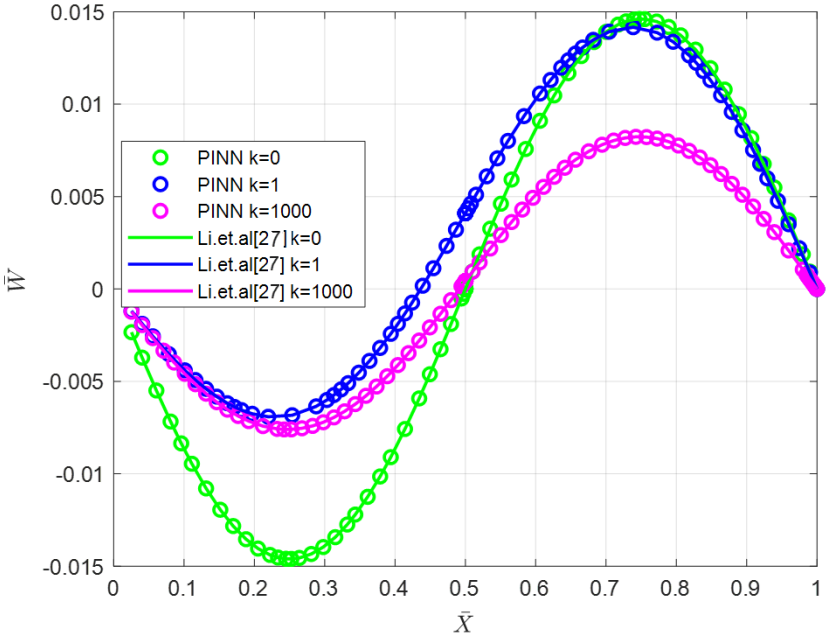

Figure 12. Normalized deformation of a simply supported FG beam with various values of the axially functionally graded index (*k*) (*ζ*=0.03 and a piecewise distributed force $\bar{q} = 10$ applied at midpoint). For comparison the results of Li et al. [27] are presented

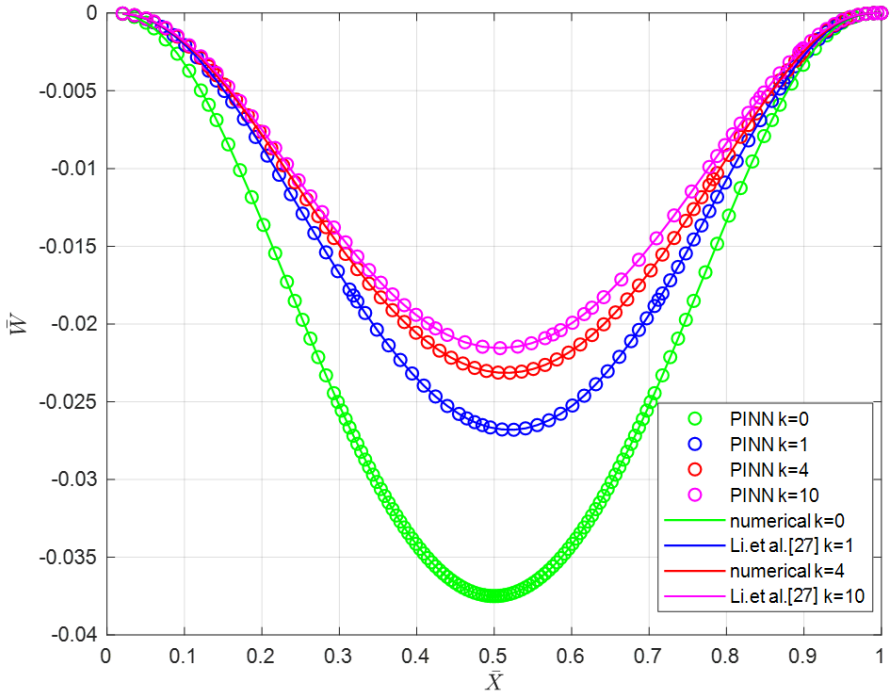

Figure 13. Normalized deflection of a clamped–clamped FG beam with different *k* values under uniform distributed load ($\bar{q} = 10$ and *ζ*=0.03), results are compared to Li et al. [27]

In Figure 13 and Figure 14 the PINN and the reported results by Li et al. [27] for axial clamped FG nano-beam are compared. Moreover, numerical results are also included to make the comparison more reliable. In Figure 13 the influence of *k* for axially nano-beam is illustrated, the obtained results closely match those reported by Li et al. [27]. As its shown by increasing the power law index, the beam deflection decreases, that's due to the fact that by

increase of power law index (*k*) the effective Young's modulus increases and will cause higher stiffness.

Figure 14 shows the deflection of axial FG nano clamped-clamped beam under uniform loading. Results of Li et al. [27] together with numerical solutions are also included which are in good agreement with the PINN predictions. Comparing the maximum deflection for the considered ζ, it is obvious that the beam stiffness increases by increasing the ζ which indicates that by increasing the value of external lengths of size-dependent nano-beams, results in decreasing the deflection.

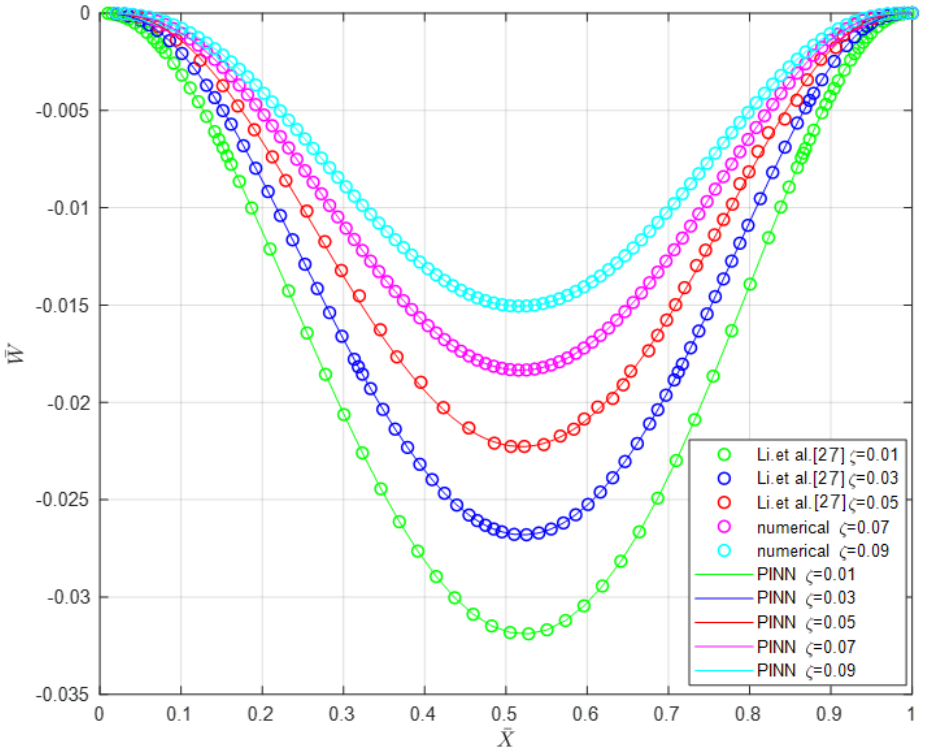

Figure 14. Normalized deflection of a clamped–clamped FG beam with various ζ values under uniformly distributed load ($\bar{q} = 10$, k=1), results are compared to Li et al. [27]

The examples provided focused on homogeneous and axial FG nano-beams under various boundary conditions and loading scenarios. In all cases, the predictions made by PINNs closely matched the analytical or numerical reference solutions, demonstrating the accuracy of the proposed PINN approach. The following examples will investigate 2D FG nano-beams.

As demonstrated in Figure 15, the effects of the material length scale parameter on the deflection of a Clamped-Free 2D nano-FG beam under a uniformly distributed load is shown. The results indicate that increasing the material length scale parameter leads to hardening effects in the beam, resulting in a decrease in maximum deflection.

In Figure 16 the bending moment of a 2D FGM nano-beam is investigated under a uniformly distributed loading and simply supported ends boundary condition, results of PINN are compatible with numerical method and agree well. It is shown that the bending moment like deflections decreases by increasing the value of ζ, therefore by choosing a proper material length scale parameter the value of bending moment and deflection is controlled.

In Figure 17, the effects of the material length scale parameter on the deflection of a simply supported 2D nano-FG beam under a sinusoidal load are investigated. The results indicate that increasing the material length scale parameter leads to hardening effects in the beam, resulting in a decrease in maximum deflection.

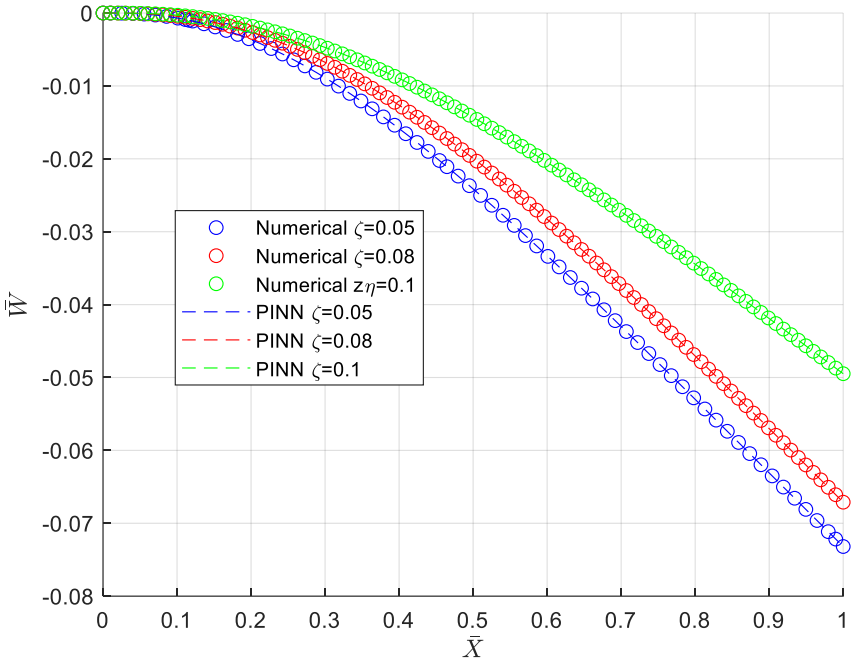

Figure 15. Normalized deflection of two dimensionally FGM nano-beam under uniformly distributed load with Clamped-Free boundary condition for different values of material length scale parameter (ζ) (*k*=2 , *β*=1 , *τ*=0.05 and $\bar{q} = 1$)

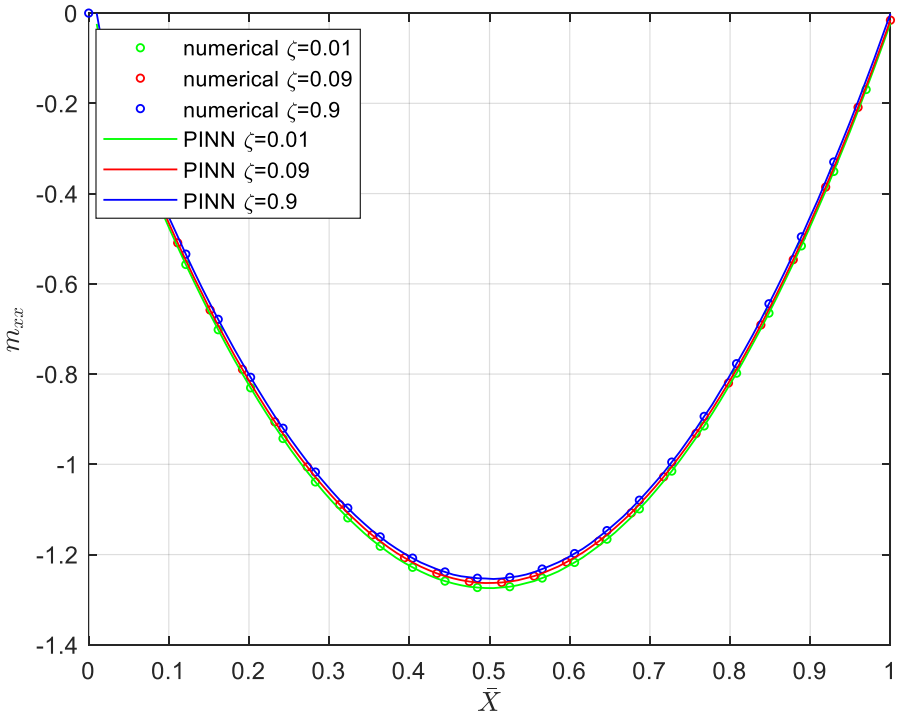

Figure 16.The bending moment of two dimensionally FGM nano-beam under uniformly distributed load with simply supported-simply supported boundary condition for different values of material length scale parameter (ζ) (*k*= *β*=1 , *τ*=0.05 and $\bar{q} = 10$)

Figure 18 shows the effect of material distribution in the z direction (β) on the deflection of a 2D simply supported FG nano-beam under a sinusoidal load. As expected, due to asymmetry in the material properties along the length direction, the deflection pattern is not symmetrical with respect to the beam's midpoint. The maximum deflection occurs at a point on the right side of the midpoint. This is because the metal constituent on the right side of the beam has a lower elastic modulus, resulting in lower beam stiffness in that region. As β increases, the beam stiffness also increases, causing the maximum deflection to decrease and shift towards the center point.

Figure 19 illustrates the maximum deflection of a simply supported 2D FG nano-beam under a sinusoidal load for different values of the length scale parameters (ζ) and nonlocal parameter (τ). The results show that the bending stiffness of the beam increases (deflection decreases) with an increase in ζ and a decrease in τ. In other words, increasing ζ has a hardening effect, while increasing τ has a softening effect on the stiffness of the beam.

Figure 20 shows the effect of boundary conditions and the power-law index (k) on the maximum deflection of a FGM nano-beam under a sinusoidal load. For all considered boundary conditions, the maximum deflection decreases with an increase in the power-law index. In the case of a cantilever beam (C-F), as the applied load increases, the beam's deflection might unreasonably exceed the beam's length. To address this, the beam has been modelled with a reduced load to ensure that the deflection remains within a reasonable range Figure 20-b. However, for other boundary conditions (Figure 20-a), this adjustment is unnecessary. To better evaluate the deflection values in these cases, the beam has been modelled with a higher applied load.

Additionally, it's shown that boundary conditions have a significant effect on maximum deflection of beam. The beam with clamped boundary conditions has the lowest deflection due to the fixed points, while the clamped – free beam has the highest deflection because of free moving at the end of the beam.

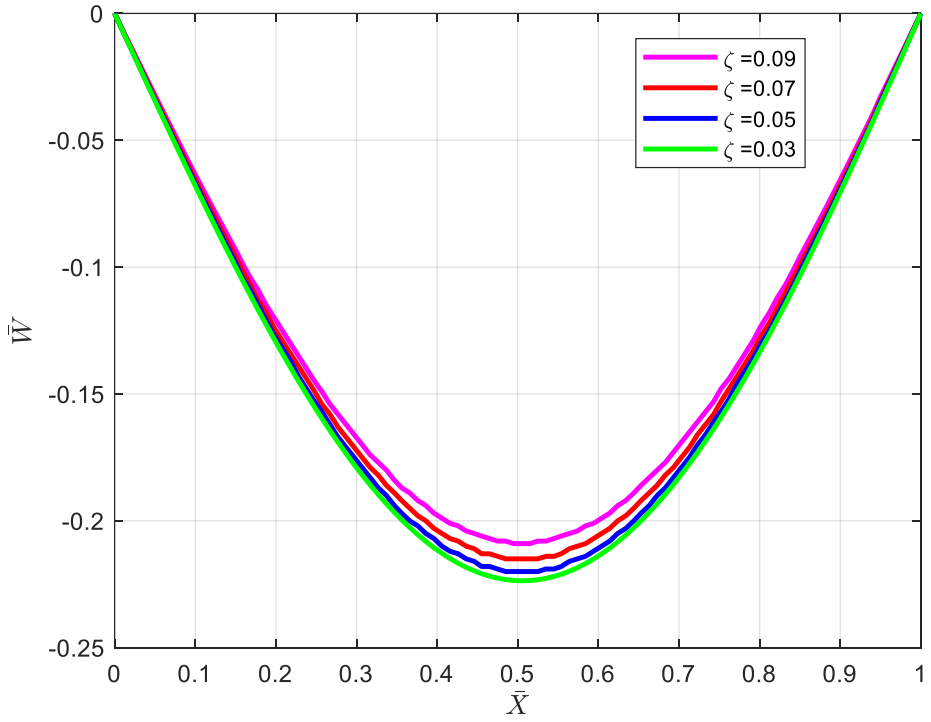

Figure 17. Normalized deflection of two dimensionally FGM nano-beam under sinusoidal distributed load with simply supported - simply supported boundary condition for different values of length scale material parameter (ζ) (k=1, β=2, τ=0)

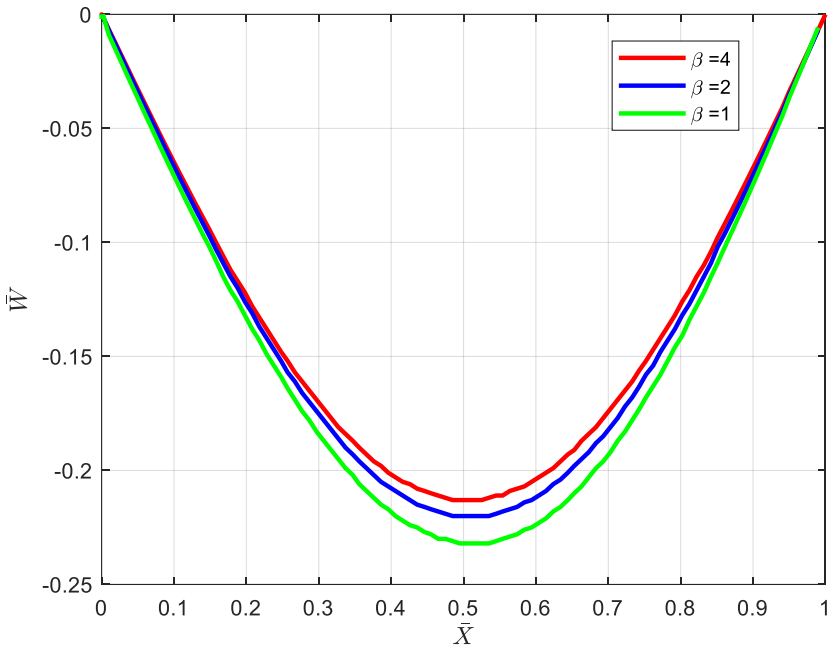

Figure 18. Normalized deflection of two dimensionally FGM nano-beam under sinusoidal distributed load $\bar{q} = 20\,sin(\pi x)$ with simply supported-simply supported boundary condition for different values of power law index of *z* direction (*β*) (*k*=2 and *ζ*=0.05, *τ*=0)

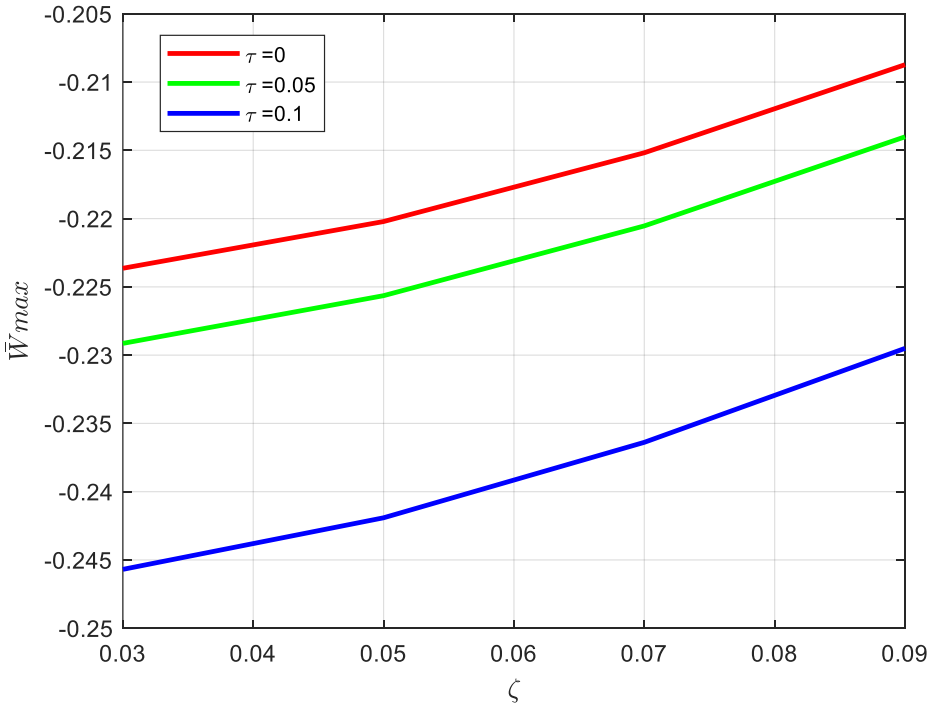

Figure 19. Maximum deflection of a simply supported 2D FG nano-beam under distributed transverse load respected to *ζ* with various value of *τ* ($\bar{q} = 20\sin(\pi x)$, *k* =1 and *β*=2).

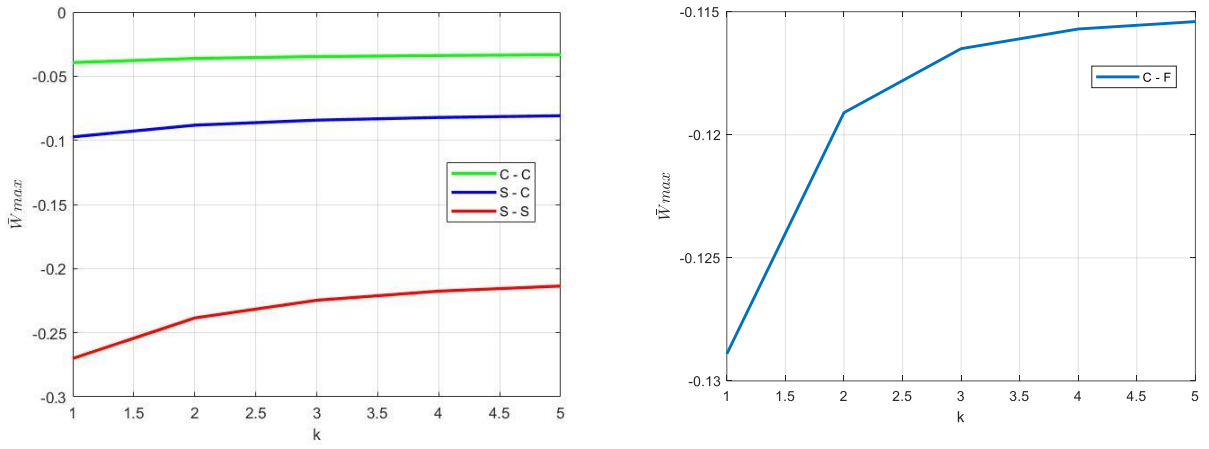

(a) **(b)**

Figure 20. Maximum normalized deflection of a FGM nano-beam as a function of the power-law index *k* with ζ=τ=0.05 , β=1 for a) simply supported–simply support (S-S), Simply support–clamped (S–C) and clamped-clamped (C-C) for higher loads ($\bar{q} = 20\sin(\pi x)$). b) Clamped-Free boundary condition with smaller load $\bar{q} = 2\sin(\pi x)$

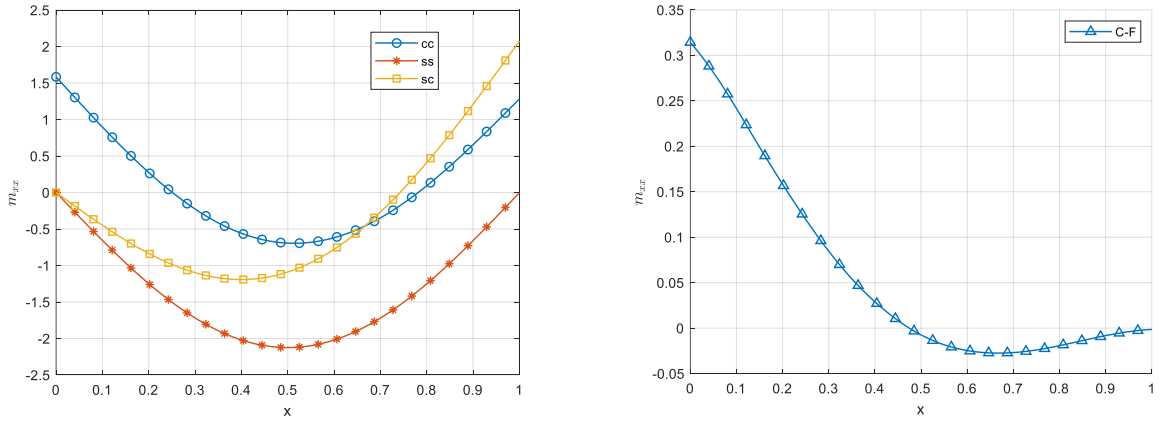

(a) **(b)**

Figure 21. The effect of boundary conditions on bending moment of a nano-beam ($\bar{q} = 20\sin(\pi x)$, ζ=τ=0.05 , k=β=1) for a) simply supported–simply support (S-S), Simply support–clamped (S–C) and clamped-clamped (C-C) for higher loads ($\bar{q} = 20\sin(\pi x)$). b) Clamped-Free boundary condition with smaller load $\bar{q} = 2\sin(\pi x)$

Figure 21-a shows the bending moments Eq. (26) versus the length of the nano-beam for different boundary conditions under sinusoidal distributed loading which shows that for simply supported boundary conditions at both ends, the moment starts and ends at zero value due to satisfying the moment condition Eq. (30), but in general the moment will vary depending on the applied loads or geometry of beam. The same happens at the start point of

simply supported –clamped boundary conditions which is zero. For a clamped-clamped boundary condition, the boundary condition ensure that the bending moment is non-zero at both ends unless the beam is uniformly loaded without any variation. Figure 21-b illustrates the bending moment for cantilever nano-beam Clamped- Free boundary conditions, where the bending moment is zero at the free end boundary condition due to satisfying Eq. (28), The bending moment gradually decreases from the clamped end to the free end.

Figure 22 represents the influence of the power-law index through length of the beam ζ for different variations of thickness power-law index β on the maximum deflection of a 2D FG nano-beam. Increasing β has a hardening effect, consequently decreasing the beam's deflection. Both power-law indexes cause decrease in beam dimensionless deflection which brings the fact that choosing proper power-law indexes the beam deflection can be controlled.

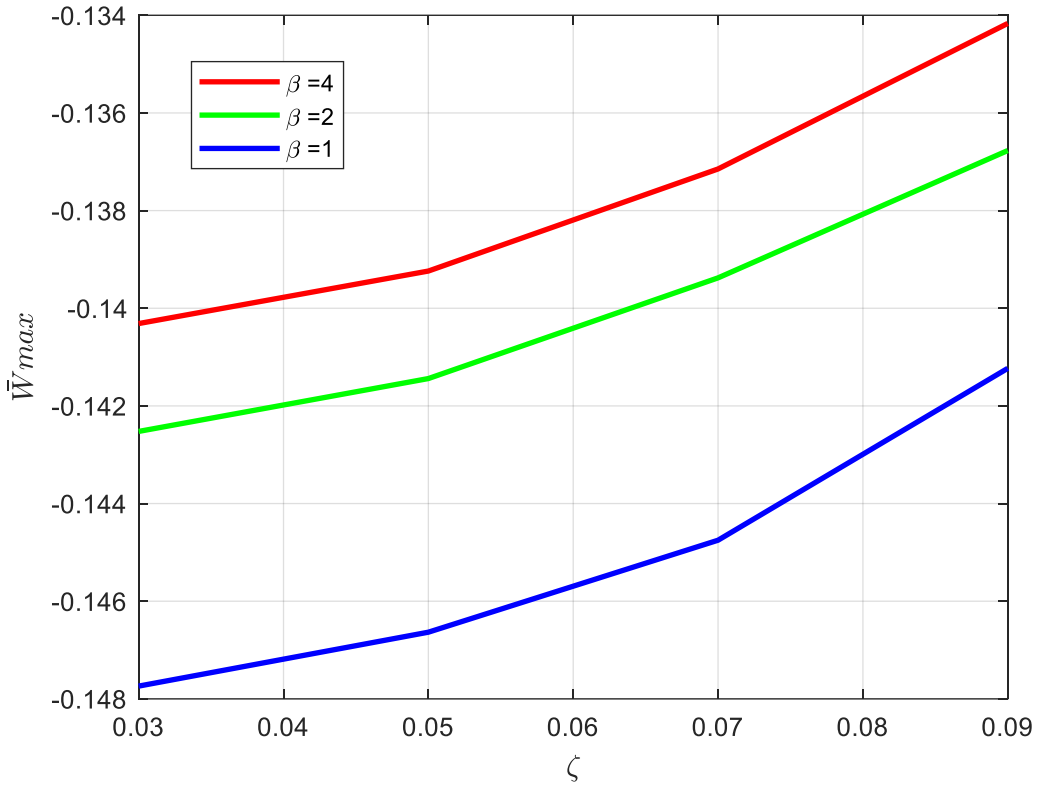

Figure 22. Maximum normalized deflection of a simply supported-simply supported 2D FGM nano-beam versus ζ with various values of β (k=1, τ=0 and $\bar{q} = 10$).

As demonstrated in Figure 23, under simply supported boundary conditions of both ends and uniformly distributed load, the bending moment Eq. (26) of a nano-beam is shown to be influenced by the power law index and non-local strain gradient parameters. It can be inferred that an increase in the power law index results in a decrease in the bending moment. As with deflections, the increase of material length scale parameter (ζ) results in decrease of the bending moment and also it can be implied that by decreasing the value of nonlocal parameter (τ), the bending moment decreases.

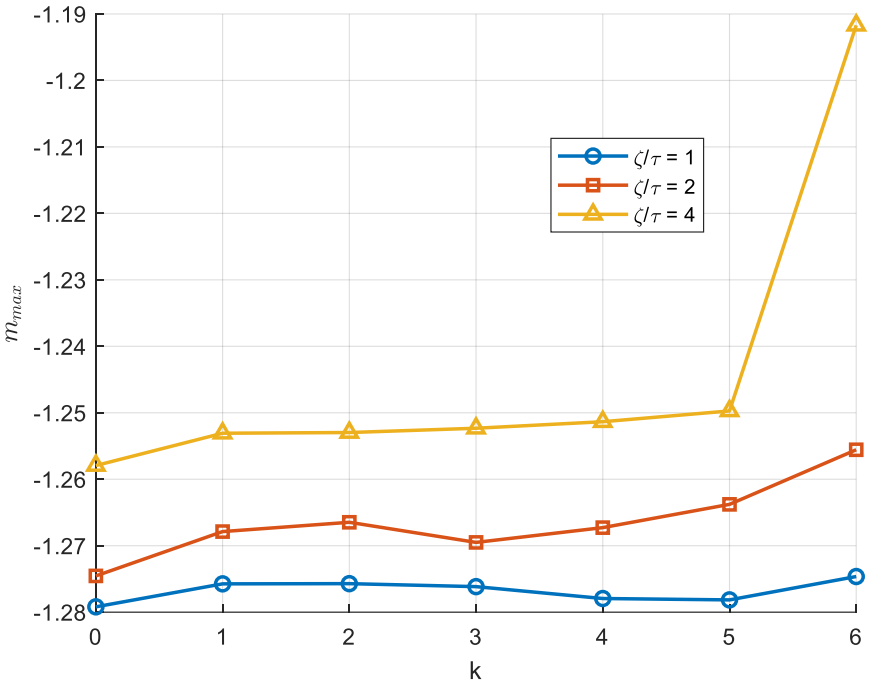

Figure 23. Maximum normalized bending moment of a simply supported-simply supported FGM nano-beam versus *k* with various values of ζ/τ ($\bar{q} = 10$, θ=1).

6. Conclusion

In this paper, PINN is employed to analyze the bending behavior of a 2D FG nano-beam using nonlocal strain gradient theory. The material properties of the beam are considered to vary through the thickness and length, creating a two-dimensional FG beam. The governing equations were derived using Hamilton's principle and nonlocal strain gradient theory. Strain gradient and nonlocal parameters are included to simultaneously account for the importance of the strain gradient stress field and the effect of the nonlocal elastic stress field on deformation.

The governing equation, a high-order variable coefficient differential equation, is solved using the PINN method. In this approach, a neural network approximates the beam deflection, and the network parameters are tuned to minimize the corresponding loss function. The PINN predictions are compared and validated against available reference solutions for homogeneous and axially FG nano-beam. The results demonstrate the accuracy and applicability of PINN for bending analysis of FG nano-beams.

Furthermore, the effects of various parameters such as material distribution, boundary conditions, loading scenarios, length scale parameters and the nonlocal parameter on the bending behavior of the 2D FG nano-beam are investigated. The results show that changes in the through-length and thickness distribution of the material properties can affect the bending of the beam. Thus, these properties can be controlled and optimized for different engineering applications.

Additionally, various types of loadings and boundary conditions are considered for the bending problem. The results indicate that increasing the material length scale parameter (ζ), power-law indexes (k, β), reduces the maximum deflection, thereby increasing the resistance of the small-scale beam against deflection. Conversely, increasing the value of the nonlocal parameter (τ) leads to an increase in deflection.

The findings confirm the applicability of PINN for solving higher-order partial differential equations with variable coefficients, which are considered a complex class of differential equations to solve. This study addresses the existing literature gap concerning the application of the PINN method for nano-mechanics using nonlocal strain gradient theory, with a particular focus on bi-directional FGM beams. The utilisation of FGM nano-beams is predominantly observed in engineering applications that demand a high degree of sensitivity, such as MEMS/NEMS systems.

Appendix A

The procedure to obtain Eqs. (12) and (13) is presented in this section. The force resultant and the bending moment of a FGM nano-beam is obtained from:

$$N_{xx} = \int t_{xx}\, dzdy \tag{37}$$

$$M_{xx} = \int z t_{xx}\, dzdy \tag{38}$$

By substituting ε_{xx} from Eq. (3) into Eq. (9), t_{xx} will take the form as:

$$(1-(ea)^2\frac{\partial^2}{\partial x^2})t_{xx} = E(x,z)(\frac{\partial u}{\partial x} - z\frac{\partial^2 w}{\partial x^2}) - l^2\frac{\partial}{\partial x}(E(x,z)\frac{\partial}{\partial x}(\frac{\partial u}{\partial x} - z\frac{\partial^2 w}{\partial x^2})) \tag{39}$$

By completing some relevant mathematical simplifying on the Eq. (39):

$$(1-(ea)^2\frac{\partial^2}{\partial x^2})t_{xx} = E(x,z)(\frac{\partial u}{\partial x} - z\frac{\partial^2 w}{\partial x^2}) - l^2\Big(\frac{\partial E(x,z)}{\partial x}(\frac{\partial^2 u}{\partial x^2} - z\frac{\partial^3 w}{\partial x^3}) + E(x,z)(\frac{\partial^3 u}{\partial x^3} - z\frac{\partial^4 w}{\partial x^4})\Big) \tag{40}$$

Substituting Eq. (40) into Eqs. (37) and (38):

$$N_{xx} = (ea)^2\frac{\partial^2 N_{xx}}{\partial x^2} + \int\left(E(x,z)(\frac{\partial u}{\partial x} - z\frac{\partial^2 w}{\partial x^2}) - l^2\Big(\frac{\partial E(x,z)}{\partial x}(\frac{\partial^2 u}{\partial x^2} - z\frac{\partial^3 w}{\partial x^3}) + E(x,z)(\frac{\partial^3 u}{\partial x^3} - z\frac{\partial^4 w}{\partial x^4})\Big)\right)dzdy \tag{41}$$

$$M_{xx} = (ea)^2\frac{\partial^2 M_{xx}}{\partial x^2} + \int z\left(E(x,z)(\frac{\partial u}{\partial x} - z\frac{\partial^2 w}{\partial x^2}) - l^2\Big(\frac{\partial E(x,z)}{\partial x}(\frac{\partial^2 u}{\partial x^2} - z\frac{\partial^3 w}{\partial x^3}) + E(x,z)(\frac{\partial^3 u}{\partial x^3} - z\frac{\partial^4 w}{\partial x^4})\Big)\right)dzdy \tag{42}$$

Substituting stiffness coefficients (Eq. (14)) into Eqs. (41) and (42), the force resultant and the bending moment of a FGM nano-beam is derived:

$$N_{xx} = (ea)^2\frac{\partial^2 N_{xx}}{\partial x^2} + A_{11}\frac{\partial u}{\partial x} - B_{11}\frac{\partial^2 w}{\partial x^2} - l^2(A_{11}\frac{\partial^3 u}{\partial x^3} - B_{11}\frac{\partial^4 w}{\partial x^4} + \frac{\partial A_{11}}{\partial x}\frac{\partial^2 u}{\partial x^2} - \frac{\partial B_{11}}{\partial x}\frac{\partial^3 w}{\partial x^3}) \tag{43}$$

$$M_{xx} = (ea)^2\frac{\partial^2 M_{xx}}{\partial x^2} + B_{11}\frac{\partial u}{\partial x} - D_{11}\frac{\partial^2 w}{\partial x^2} - l^2(B_{11}\frac{\partial^3 u}{\partial x^3} - D_{11}\frac{\partial^4 w}{\partial x^4} + \frac{\partial B_{11}}{\partial x}\frac{\partial^2 u}{\partial x^2} - \frac{\partial D_{11}}{\partial x}\frac{\partial^3 w}{\partial x^3}) \tag{44}$$

Appendix B.

In this section the procedure to derive Eqs. (15) and (16) from Eqs. (12) and (13) is explained. By employing Eq. (10), (11) the Eqs. (12) and (13) can be expressed as:

$$N_{xx} = (ea)^2\frac{\partial}{\partial x}(f) + A_{11}\frac{\partial u}{\partial x} - B_{11}\frac{\partial^2 w}{\partial x^2} - l^2(A_{11}\frac{\partial^3 u}{\partial x^3} - B_{11}\frac{\partial^4 w}{\partial x^4} + \frac{\partial A_{11}}{\partial x}\frac{\partial^2 u}{\partial x^2} - \frac{\partial B_{11}}{\partial x}\frac{\partial^3 w}{\partial x^3}) \tag{45}$$

$$M_{xx} = (ea)^2\left(q + \overline{N}\frac{\partial^2 w}{\partial x^2}\right) + B_{11}\frac{\partial u}{\partial x} - D_{11}\frac{\partial^2 w}{\partial x^2} - l^2(B_{11}\frac{\partial^3 u}{\partial x^3} - D_{11}\frac{\partial^4 w}{\partial x^4} + \frac{\partial B_{11}}{\partial x}\frac{\partial^2 u}{\partial x^2} - \frac{\partial D_{11}}{\partial x}\frac{\partial^3 w}{\partial x^3}) \tag{46}$$

Now by substituting these equations into equilibrium Eqs. (10) and (11), the governing equations can be derived as:

$$\delta u: -(1-(ea)^2\frac{\partial^2}{\partial x^2})f + \frac{\partial}{\partial x}\left(A_{11}\frac{\partial u}{\partial x} - B_{11}\frac{\partial^2 w}{\partial x^2} - l^2(A_{11}\frac{\partial^3 u}{\partial x^3} - B_{11}\frac{\partial^4 w}{\partial x^4} + \frac{\partial A_{11}}{\partial x}\frac{\partial^2 u}{\partial x^2} - \frac{\partial B_{11}}{\partial x}\frac{\partial^3 w}{\partial x^3})\right) = 0 \tag{47}$$

$$\delta w: -(1-(ea)^2\frac{\partial^2}{\partial x^2})\left(\overline{N}\frac{\partial^2 w}{\partial x^2} + q\right) + \frac{\partial^2}{\partial x^2}\left(+B_{11}\frac{\partial u}{\partial x} - D_{11}\frac{\partial^2 w}{\partial x^2} - l^2(B_{11}\frac{\partial^3 u}{\partial x^3} - D_{11}\frac{\partial^4 w}{\partial x^4} + \frac{\partial B_{11}}{\partial x}\frac{\partial^2 u}{\partial x^2} - \frac{\partial D_{11}}{\partial x}\frac{\partial^3 w}{\partial x^3})\right) = 0 \tag{48}$$

References

[1] A. Fallah, M. M. Aghdam, Physics-informed neural network for bending and free vibration analysis of three-dimensional functionally graded porous beam resting on elastic foundation, *Engineering with Computers*, 2023/03/13, 2023.

[2] M. Arabzadeh-Ziari, M. Mohammadimehr, E. Arabzadeh-Ziari, M. Asgari, Deflection, buckling and vibration analyses for a sandwich nanocomposite structure with foam core reinforced with GPLs and SMAs based on TSDBT, *Journal of Computational Applied Mechanics*, Vol. 55, No. 2, pp. 289-321, 2024.

[3] A. A. Monajemi, M. Mohammadimehr, F. Bargozini, Dynamic analysis of a spinning visco-elastic FG graphene platelets reinforced nanocomposite sandwich cylindrical shell with MRE core, *Acta Mechanica*, pp. 1-34, 2024.

[4] F. Shirdelan, M. Mohammadimehr, F. Bargozini, Control and vibration analyses of a sandwich doubly curved micro-composite shell with honeycomb, truss, and corrugated cores based on the fourth-order shear deformation theory, *Applied Mathematics and Mechanics*, Vol. 45, No. 10, pp. 1773-1790, 2024.

[5] M. Mohammadimehr, The effect of a nonlocal stress-strain elasticity theory on the vibration analysis of Timoshenko sandwich beam theory, *Advances in nano research*, Vol. 17, No. 3, pp. 275-284, 2024.

[6] A. C. Eringen, On differential equations of nonlocal elasticity and solutions of screw dislocation and surface waves, 1983.

[7] M. Z. Nejad, A. Hadi, A. Rastgoo, Buckling analysis of arbitrary two-directional functionally graded Euler–Bernoulli nano-beams based on nonlocal elasticity theory, *International Journal of Engineering Science*, Vol. 103, pp. 1-10, 2016.

[8] J. Reddy, Microstructure-dependent couple stress theories of functionally graded beams, *Journal of the Mechanics and Physics of Solids*, Vol. 59, No. 11, pp. 2382-2399, 2011.

[9] Bending, buckling, and vibration of micro/nanobeams by hybrid nonlocal beam model, *engineering mechanic* 2009.

[10] The small length scale effect for a non-local cantilever beam: a paradox solved, *IOPscience*, Vol. 19, 2008.

[11] U. Güven, A generalized nonlocal elasticity solution for the propagation of longitudinal stress waves in bars, *Elsevier*, Vol. 45, 2014.

[12] Bending, buckling and vibration of axially functionally graded beamsbased on nonlocal strain gradient theory, *Elsevier-composite structures*, pp. 250-265, 2017.

[13] Nonlinear bending and free vibration analyses of nonlocal strain gradient beams made of functionally graded material, *Elsevier*, Vol. 107, pp. 77-97, 2016.

[14] M. Şimşek, Nonlinear free vibration of a functionally graded nanobeam using nonlocal strain gradient theory and a novel Hamiltonian approach, *elsevier*, Vol. 105, pp. 12-27, 2016.

[15] Numerical solution of partial differential equations: finite difference methods, *Oxford University Press*, 1995.

[16] Nonconservative stability problems via generalized differential quadrature method, *elsevier*, Vol. 315, 2008.

[17] Physics-Informed Neural Networks: A Deep Learning Framework for Solving Forward and Inverse Problems Involving Nonlinear Partial Differential Equations, *Journal of computational physics*, Vol. 738, pp. 686-707, 2019.

[18] A. Fallah, M. M. Aghdam, *Physics-Informed Neural Network for Solution of Nonlinear Differential Equations*, in: R. N. Jazar, L. Dai, *Nonlinear Approaches in Engineering Application: Automotive Engineering Problems*, Eds., pp. 163-178, Cham: Springer Nature Switzerland, 2024.

[19] Active training of physics-informed neural networks to aggregate and interpolate parametric solutions to the Navier-Stokes equations, *Journal of Computational Physics-ELSEVIER*, pp. 438, 2021.

[20] Learning the physics of pattern formation from images. Phys Rev Lett *PHYSICS REVIEW LETTERS*, 2020.

[21] A physics-informed deep learning framework for inversion and surrogate modeling in solid mechanics, *Elsevier*, Vol. 379, 2021.

[22] A recurrent neural network-accelerated multi-scale model for elasto-plastic heterogeneous materials subjected to random cyclic and non-proportional loading paths, *elsevier*, Vol. 369, 2020.

[23] M. Bazmara, M. Silani, M. Mianroodi, Physics-informed neural networks for nonlinear bending of 3D functionally graded beam, in *Proceeding of*, Elsevier, pp. 152-162.

[24] Deep autoencoder based energy method for the bending, vibration, and buckling analysis of Kirchhof plates with transfer learning, *Eur journal mechanics*, 2021.

[25] O. Kianian, S. Sarrami, B. Movahedian, M. Azhari, PINN-based forward and inverse bending analysis of nanobeams on a three-parameter nonlinear elastic foundation including hardening and softening effect using nonlocal elasticity theory, *Engineering with Computers*, pp. 1-27, 2024.

[26] M. S. Es-haghi, M. Bamdad, C. Anitescu, Y. Wang, X. Zhuang, T. Rabczuk, Deepnetbeam: A Framework for the Analysis of Functionally Graded Porous Beams, *Available at SSRN 4846935*.

[27] X. Li, L. Li, Y. Hu, Z. Ding, W. Deng, Bending, buckling and vibration of axially functionally graded beams based on nonlocal strain gradient theory
Composite Structures, Vol. 165, pp. 250-265, 2017.

[28] X. Li, L. Li, Y. Hu, Nonlinear bending of a two-dimensionally functionally graded beam, *Composite Structures*, Vol. 185, pp. 1049-1061, 2018.

[29] C. Lim, G. Zhang, J. Reddy, A higher-order nonlocal elasticity and strain gradient theory and its applications in wave propagation, *Journal of the Mechanics and Physics of Solids*, Vol. 78, pp. 298-313, 2015.

[30] D. Polyzos, D. Fotiadis, Derivation of Mindlin's first and second strain gradient elastic theory via simple lattice and continuum models, *International Journal of Solids and Structures*, Vol. 49, No. 3-4, pp. 470-480, 2012.

[31] E. C. Aifantis, On the role of gradients in the localization of deformation and fracture, *International Journal of Engineering Science*, Vol. 30, No. 10, pp. 1279-1299, 1992.

[32] S. Abrate, Functionally graded plates behave like homogeneous plates, *Composites part B: engineering*, Vol. 39, No. 1, pp. 151-158, 2008.

[33] Z. Luo, Q. Shi, L. Wang, Size-Dependent Mechanical Behaviors of Defective FGM Nanobeam Subjected to Random Loading, *Applied Sciences*, Vol. 12, No. 19, pp. 9896, 2022.

[34] A. Fallah, M. Aghdam, Nonlinear free vibration and post-buckling analysis of functionally graded beams on nonlinear elastic foundation, *European Journal of Mechanics-A/Solids*, Vol. 30, No. 4, pp. 571-583, 2011.

[35] A. Fallah, M. Aghdam, Thermo-mechanical buckling and nonlinear free vibration analysis of functionally graded beams on nonlinear elastic foundation, *Composites Part B: Engineering*, Vol. 43, No. 3, pp. 1523-1530, 2012.

[36] S. Cuomo, V. S. Di Cola, F. Giampaolo, G. Rozza, M. Raissi, F. Piccialli, Scientific machine learning through physics–informed neural networks: Where we are and what's next, *Journal of Scientific Computing*, Vol. 92, No. 3, pp. 88, 2022.

[37] M. Bazmara, M. Mianroodi, M. Silani, Application of physics-informed neural networks for nonlinear buckling analysis of beams, *Acta Mechanica Sinica*, Vol. 39, No. 6, pp. 422438, 2023.

[38] W. Li, M. Z. Bazant, J. Zhu, A physics-guided neural network framework for elastic plates: Comparison of governing equations-based and energy-based approaches, *Computer Methods in Applied Mechanics and Engineering*, Vol. 383, pp. 113933, 2021.

[39] K.-I. Funahashi, On the approximate realization of continuous mappings by neural networks, *Neural networks*, Vol. 2, No. 3, pp. 183-192, 1989.

[40] X. Zhuang, H. Guo, N. Alajlan, H. Zhu, T. Rabczuk, Deep autoencoder based energy method for the bending, vibration, and buckling analysis of Kirchhoff plates with transfer learning, *European Journal of Mechanics-A/Solids*, Vol. 87, pp. 104225, 2021.

[41] H. N. Mhaskar, T. Poggio, Deep vs. shallow networks: An approximation theory perspective, *Analysis and Applications*, Vol. 14, No. 06, pp. 829-848, 2016.

[42] L. Lu, X. Meng, Z. Mao, G. E. Karniadakis, DeepXDE: A deep learning library for solving differential equations, *SIAM review*, Vol. 63, No. 1, pp. 208-228, 2021.

[43] M. Abadi, P. Barham, J. Chen, Z. Chen, A. Davis, J. Dean, M. Devin, S. Ghemawat, G. Irving, M. Isard, {TensorFlow}: a system for {Large-Scale} machine learning, in *Proceeding of*, 265-283.

[44] A. Paszke, S. Gross, S. Chintala, G. Chanan, E. Yang, Z. DeVito, Z. Lin, A. Desmaison, L. Antiga, A. Lerer, Automatic differentiation in pytorch, 2017.

[45] J. Bergstra, O. Breuleux, F. Bastien, P. Lamblin, R. Pascanu, G. Desjardins, J. P. Turian, D. Warde-Farley, Y. Bengio, Theano: A CPU and GPU Math Compiler in Python, in *Proceeding of*, 18-24.

[46] T. Chen, M. Li, Y. Li, M. Lin, N. Wang, M. Wang, T. Xiao, B. Xu, C. Zhang, Z. Zhang, Mxnet: A flexible and efficient machine learning library for heterogeneous distributed systems, *arXiv preprint arXiv:1512.01274*, 2015.

[47] D. P. Kingma, J. Ba, Adam: A method for stochastic optimization, *arXiv preprint arXiv:1412.6980*, 2014.